



POLITECNICO MILANO 1863

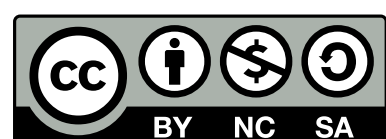
Preliminary Design, Modelling and Comparison of Green and Toxic Rocket Engines For Kick Stages Applications

Team: **SMB(G-S)**

P. Code	Surname	Name
10913819	Albiñana Burdiel	Carlos
10882032	Aranda Romero	Fernando
10530771	Aufiero	Luca
10911047	Balest	Alice
10663873	Degener	Martín
10460186	Prudenzi	Luca
10663664	Sánchez	Amanda
10599185	Sangiorgi	Filippo
10620170	Scimone	Dario

Space Propulsion
Prof: F. Maggi
M.Sc Space Engineering
Academic Year 2022-2023

This work is licensed under a Creative Commons
“Attribution-NonCommercial-ShareAlike 4.0 International” license.



Abstract

This report summarises the design, analysis and comparison of two pressure-fed non-throttling liquid rocket engine (LRE) propulsion system for use as orbital transfer stages. Two propellant couples are evaluated to provide a ΔV of 2500 m/s with 250 kg of inert mass. The first system is designed for use with Monomethylhydrazine (MMH)-Nitrogen Tetroxide and the second one for operation with $RP - 1-98\% H_2O_2$. The thrust chamber is designed to be produced in a single block using additive manufacturing. The analysis is carried out for three thrust cases of 0.5 kN, 1kN and 2kN. A preliminary study is performed to obtain the sizing of the combustion and propellant systems, as well as a modelling of the nozzle using Rao approximation. Regenerative cooling is studied together with thermal protection coating post-processing to assure the survivability of the engine. This work provides the data needed to perform a trade-off analysis based on different mission drivers.

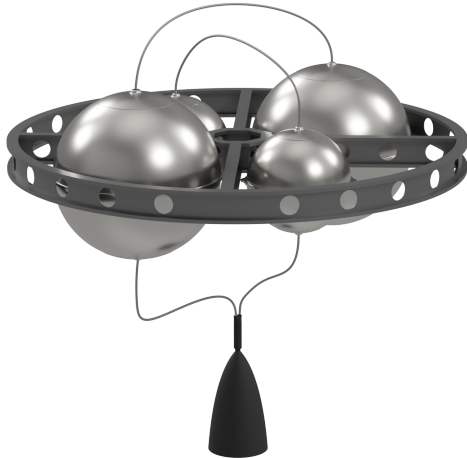


Figure 1: CAD Model of the green nominal thruster



Figure 2: CAD Model of the toxic nominal thruster

Contents

1 Literature Review	1
1.1 Kick stages	1
1.2 Green Propellant	1
1.2.1 Fuel Selection	2
1.2.2 Combustion Chamber Pressure Selection	3
1.3 Toxic Propellant	4
1.3.1 Combustion Chamber Pressure Selection	4
1.4 Materials and manufacturing	5
1.4.1 Thrust chamber	5
1.4.2 Green Propellant Tanks	5
1.4.3 Toxic Propellants Tanks	6
1.4.4 Additive Manufacturing	7
2 Engines Modelling	8
2.1 Nozzle Design	8
2.1.1 CEAM Analysis	9
2.1.2 Expansion Ratio Optimization	10
2.1.3 Conic Nozzle	11
2.1.4 Rao Approximation	11
2.1.5 Optimization & Results	12
2.2 Combustion Chamber Model	13
2.2.1 Shapiro model	13
2.2.2 Selection of contraction ratio	14
2.2.3 Results	15
2.3 Injectors	15
2.3.1 MMH-NTO injectors	15
2.3.2 H ₂ O ₂ -RP1 injectors	15
2.3.3 Results	16
2.4 Pressurization System	17
2.4.1 Pressure Losses	17
3 Thermal Analysis	20
3.1 Regenerative Cooling Thermal Analysis	20
3.2 Coating Design and Validation	20
3.3 Results Discussion	21
A CAD Modelling	30
B Graphical Approaches	32
B.1 Rao Approximation	32
C CEAM Analysis	33
C.1 Chemical Composition At Exit Section	34
C.2 Equilibrium, Frozen and Bray Models	35
C.2.1 Nominal Case	35
C.2.2 Halved Case	37
C.2.3 Doubled Case	38
D Pressure cascade: full analysis	40

List of Figures

1	CAD Model of the green nominal thruster	i
2	CAD Model of the toxic nominal thruster	i
1.1	Green fuel trade-off	3
1.2	P_{CC} vs Thrust trend in orbital Hydrazine and NTO bipropellant engines	5
2.1	Workflow followed for iterative design of Nozzle and Combustion Chamber	8
2.2	Green couple - $\frac{O}{F}$ and ϵ trade-off	10
2.3	Toxic couple - $\frac{O}{F}$ and ϵ trade-off	10
2.4	Green couple - $I_{sp,VAC}$ at different ϵ	10
2.5	Toxic couple - $I_{sp,VAC}$ at different ϵ	10
2.6	Green couple - mass gain at different ϵ	12
2.7	Toxic couple - mass gain at different ϵ	12
2.8	Green couple - M optimization	14
2.9	Toxic couple - M optimization	14
2.10	Green couple - ϵ_c , M_{CC} and L_{CC} trade-off	15
2.11	Toxic couple - ϵ_c , M_{CC} and L_{CC} trade-off	15
2.12	Toxic couple injection plate	16
2.13	Green couple injection plate	17
2.14	Pressure cascade - Green nominal. Starting from the tank pressure of the propellant, the pressure jumps correspond respectively to $\Delta P_{dynamics}$, ΔP_{valve} , $\Delta P_{feeding}$, ΔP_{bed} only for H_2O_2 and $\Delta P_{injector}$	18
3.1	Coat temperature and thickness - Toxic halved	22
3.2	Wall temperature and heat flux - Toxic halved	22
3.3	Wall temperature and heat flux - Toxic nominal	22
3.4	Wall temperature and heat flux - Toxic doubled	22
3.5	Coat temperature and thickness - Green halved	22
3.6	Wall temperature and heat flux - Green halved	22
3.7	Coat temperature and thickness - Green nominal	23
3.8	Wall temperature and heat flux - Green nominal	23
3.9	Coat temperature and thickness - Green doubled	23
3.10	Wall temperature and heat flux - Green doubled	23
A.1	CAD model of the Toxic Nominal engine	30
A.2	Cutaway CAD model of the Toxic Nominal engine	30
A.3	CAD model of the Green Nominal engine	31
A.4	Cutaway CAD model of the Green Nominal engine	31
B.1	Efficiency of an equivalent bell nozzle as a function of percentage of an equivalent 15 deg conical nozzle	32
B.2	Limit parabola angles of an equivalent bell nozzle as a function of expansion ratio and percentage of an equivalent 15 deg conical nozzle	32

C.1	Green nominal - ϵ at different $\frac{O}{F}$	33
C.2	Toxic nominal - ϵ at different $\frac{O}{F}$	33
C.3	Green nominal - ϵ vs I_{sp}	35
C.4	Toxic nominal - ϵ vs I_{sp}	35
C.5	Green nominal - ϵ vs $I_{sp,VAC}$	35
C.6	Toxic nominal - ϵ vs $I_{sp,VAC}$	35
C.7	Green nominal - ϵ vs C_F	36
C.8	Toxic nominal - ϵ vs C_F	36
C.9	Green nominal - ϵ vs M	36
C.10	Toxic nominal - ϵ vs M	36
C.11	Green nominal - ϵ vs T	36
C.12	Toxic nominal - ϵ vs T	36
C.13	Green halved - ϵ vs I_{sp}	37
C.14	Toxic halved - ϵ vs I_{sp}	37
C.15	Green halved - ϵ vs $I_{sp,VAC}$	37
C.16	Toxic halved - ϵ vs $I_{sp,VAC}$	37
C.17	Green halved - ϵ vs C_F	37
C.18	Toxic halved - ϵ vs C_F	37
C.19	Green halved - ϵ vs M	38
C.20	Toxic halved - ϵ vs M	38
C.21	Green halved - ϵ vs T	38
C.22	Toxic halved - ϵ vs T	38
C.23	Green doubled - ϵ vs I_{sp}	38
C.24	Toxic doubled - ϵ vs I_{sp}	38
C.25	Green doubled - ϵ vs $I_{sp,VAC}$	39
C.26	Toxic doubled - ϵ vs $I_{sp,VAC}$	39
C.27	Green doubled - ϵ vs C_F	39
C.28	Toxic doubled - ϵ vs C_F	39
C.29	Green doubled - ϵ vs M	39
C.30	Toxic doubled - ϵ vs M	39
C.31	Green doubled - ϵ vs T	39
C.32	Toxic doubled - ϵ vs T	39
D.1	Pressure cascade - Toxic halved	40
D.2	Pressure cascade - Toxic nominal	40
D.3	Pressure cascade - Toxic doubled	41
D.4	Pressure cascade - Green halved	41
D.5	Pressure cascade - Green doubled	41

List of Tables

1.1	RFA OTV specification	1
1.2	Trade-off values for green propellant fuels	3
1.3	Boundary types	4
1.4	Comparison of P_{CC} and T	4
1.5	Material selection - Green case	6
1.6	Material selection - Toxic case	7
1.7	SLM800 additive manufacturing 3D printer characteristics	7

1.8	Inconel 718 post-processing techniques	7
2.1	Trade-off values for green propellant fuels	9
2.2	Nozzle results for the six different cases	13
2.3	Combustion chamber results for the six different cases	15
2.4	Injector properties for the toxic couple	16
2.5	Injector properties for the green couple	16
2.6	Pressure cascade results	18
2.7	Volume sizing results	18
2.8	Mass sizing results	19
3.1	Regenerative cooling results for the six different cases	21
3.2	Performance Datasheet comparison between the six final engines	24
C.1	Used CEAM's results	33
C.2	Chemical composition at the exit of the nozzle for the green couple in nominal condition	34
C.3	Chemical composition at the exit of the nozzle for the toxic couple in nominal condition	34
C.4	Chemical composition at the exit of the nozzle for the green couple in halved condition	34
C.5	Chemical composition at the exit of the nozzle for the toxic couple in halved condition	34
C.6	Chemical composition at the exit of the nozzle for the green couple in doubled condition	35
C.7	Chemical composition at the exit of the nozzle for the toxic couple in doubled condition	35

List of Symbols

Variable	Description	Unit
α	Divergent conic nozzle angle	deg
β	Convergent conic nozzle angle	deg
γ	Heat specific ratio	-
ΔP	Pressure loss	Pa
ΔP_{bed}	Pressure drop along the catalytic bed	Pa
$\Delta P_{dynamics}$	Dynamic Pressure Loss between Tank and Feeding Line	Pa
$\Delta P_{feeding}$	Pressure loss in feeding lines	Pa
$\Delta P_{fuel,model}$	Pressure loss between fuel tank and CC	Pa
$\Delta P_{injector}$	Pressure loss in injector	Pa
$\Delta P_{required}$	Required pressure loss for correct injector plate functioning	Pa
$\Delta P_{ox,model}$	Pressure loss between OX tank and CC	Pa
ΔP_{valve}	Pressure loss in valve	Pa
ΔT	Variation of temperature	K
ΔT_{coat}	Variation of the coating temperature	K
$\Delta T_{coolant}$	Variation of the coolant temperature	K
Δt	Time interval	s
Δv	Variation of velocity	m/s
Δx	Variation of length	m
ϵ	Expansion ratio	-
ϵ_c	Contraction ratio	-
ϵ_p	Porosity of catalytic bed	-
θ_{i-ML}	Initial Rao convergent angle for Minimum Length	deg
θ_{i-MP}	Initial Rao convergent angle for Maximum Performance	deg
θ_e	Final Rao convergent angle	deg
θ_{e-ML}	Final Rao convergent angle for Minimum Length	deg
θ_{e-MP}	Final Rao convergent angle for Maximum Performance	deg
λ	Divergent section efficiency	-
λ_{conic}	Divergent section efficiency for conic nozzle	-
λ_{dist}	Distributed friction coefficient	-
λ_{Rao-ML}	Nozzle Efficiency for Rao Minimum Length	-
λ_{Rao-MP}	Nozzle Efficiency for Rao Maximum Performance	-

Variable	Description	Unit
μ	Dynamic viscosity	$P \cdot s$
ρ	Density	kg/m^3
ρ_p	Propellant density	kg/m^3
σ_{yield}	Yield strength	N/m^2
A	Section Area	m^2
A_C	Combustion chamber Area	m^2
A_t	Throat Area	m^2
c^*	Characteristic velocity	m/s
C_D	Drag coefficient	—
C_F	Thrust coefficient	—
c_{pC}	Specific heat capacity of the coolant	J/kgK
D	Diameter	m
D_{cat}	Diameter of catalytic bed	m
D_{CC}	Combustion chamber diameter	m
D_e	Nozzle exit diameter	m
$D_{feed-FU}$	Fuel feeding line tubes diameter	m
$D_{feed-OX}$	Oxidizer feeding line tubes diameter	m
D_{inj-FU}	Fuel injector hole diameter	m
D_{inj-OX}	Oxidizer injector hole diameter	m
D_{pipe}	Diameter of pipe	m
D_t	Throat section diameter	m
I_{sp}	Specific impulse	s
I_{sp-VAC}	Vacuum specific impulse	s
K	Conductive Coefficient	—
L_{CC}	Combustion chamber length	m
L_{cat}	Length of the catalytic bed at end of feeding line	m
L_{cyl}	Length of the thermal cylinder	m
$L_{div-conv}$	Conic Nozzle convergent length	m
$L_{div-conic}$	Conic Nozzle divergent length	m
L_{pipe}	Length of pipe	m
L_{Rao-ML}	Rao nozzle divergent reference length for Minimum Length	m
L_{Rao-MP}	Rao nozzle divergent reference length for Maximum Performance	m
L^*	Combustion chamber characteristic length	m
M	Mach number	—
M_{CC}	Combustion chamber mach number	—

Variable	Description	Unit
m_{dry}	Dry mass of the pressurization system	kg
m_{fuel}	Fuel mass	kg
$m_{fuel,tank}$	Fuel tank mass	kg
m_{ox}	Oxidizer mass	kg
$m_{ox,tank}$	Oxidizer tank mass	kg
m_p	Propellant mass	kg
$m_{p,tot}$	Total mass of propellant and their tanks	kg
$m_{press,fuel}$	Mass of fuel pressurizing agent	kg
$m_{press,fuel,tank}$	Mass of fuel pressurizing agent tank	kg
$m_{press,ox}$	Mass of oxidizer pressurizing agent	kg
$m_{press,ox,tank}$	Mass of oxidizer pressurizing agent tank	kg
$m_{press,tot}$	Total mass of pressurizing agents and their tanks	kg
m_{tot}	Total mass of propellant, tanks and agents	kg
\dot{m}	Total mass of propellant, tanks and agents	kg
\dot{m}_c	Mass flow rate	kg/s
\dot{m}_p	Coolant mass flow rate	kg/s
\dot{m}_{FU}	Propellant mass flow rate	kg/s
\dot{m}_{OX}	Fuel mass flow rate	kg/s
M_m	Oxidizer mass flow rate	kg/s
$\frac{O}{F}$	Molar mass	g/mol
P_{amb}	Oxidizer to fuel ratio	—
P_{CC}	External pressure	Pa
P_e	Combustion chamber pressure	bar
P_{FU}	Exit pressure	bar
P_{fluid}	Fuel pressure	Pa
P_{inj}	Fluid pressure	Pa
P_{OX}	Pressure in injector plate	Pa
P_0	Oxidizer pressure	Pa
$P_{p,tank}$	Total pressure	Pa
$Q_{hot-gas}$	Pressure Tank	Pa
$Q_{coolant}$	Heat of hot gas	W
q	Heat of coolant	W
R	Heat Flux	W/m ²
R_{cyl}	Universal gas constant	J/molK
r_e	Cylindrical Thermal Resistance	K/W
r_i	External Radius	m
$r_{p,fluid,tank}$	Internal Radius	m
r_t	Internal Radius	m
T	Throat Radius	J/molK
	Thrust	N

Variable	Description	Unit
T_0	Total temperature	K
T_{amb}	Ambient temperature	K
T_b	Boiling Temperature	K
T_{CC}	Combustion chamber temperature	K
T_{con-1D}	One-dimensional thrust for conic nozzle	N
T_{con-2D}	Two-dimensional thrust for conic nozzle	N
$T_{ext-coat}$	Coating External Temperature	K
T_{final}	Final Temperature	K
T_{flame}	Adiabatic Flame Temperature	K
T_{sat}	Saturation Temperature	K
T/W	Thrust to weight ratio	—
t	Tank wall thickness	K
t_b	Burning time	K
V_{CC}	Combustion chamber volume	m^3
V_{gas}	Gas volume	m^3
$V_{fuel,tank}$	Volume of fuel tank	m^3
$V_{ox,tank}$	Volume of fuel tank	m^3
$V_{press,fuel,tank}$	Volume of fuel pressurizing tank	m^3
$V_{press,ox,tank}$	Volume of fuel pressurizing tank	m^3
V_{tot}	Total volume of propellant and pressurizing agents	m^3
\dot{V}_p	Gas volume	m^3/s
V_p	Propellant volume	m^3
V_{g-FU}	Nitrogen volume in the fuel tank	m^3
V_{g-OX}	Nitrogen volume in the oxidizer tank	m^3
v_{gasCC}	Gas velocity in the Combustion Chamber	m/s
v_{inj}	Velocity in the injectors	m/s

Acronyms

-	Description
AM	Additive Manufacturing
CC	Combustion Chamber
GHS	Globally Harmonized System of Classification and Labelling of Chemicals
CEAM	Chemical Equilibrium with Applications Matlab
HTP	High-Test Peroxide
RP – 1	Rocket Propellant 1
MMH	Monomethylhydrazine
NO	Nitric Acid
UDMH	Unsymmetrical Dimethyl Hydrazine
AM	Additive Manufacturing
NTO	Nitrogen Tetroxide
PTFE	Polytetrafluoroethylene
MEOP	Maximum Expected Operating Pressure

Chapter 1

Literature Review

1.1 Kick stages

The recent expansion of the space market led to the creation of a new class of spacecrafts or upper stages called *Kick Stages*. Usually developed by space launcher providers, kick stages offer increased flexibility to the end user in terms of achievable orbits.

From a Propulsion Subsystem viewpoint, various options can be found:

- **Chemical** propulsion based on **Toxic** propellants: this is the most common choice due to high performances and wide knowledge coming from historical data. As propellant, Hydrazine and its derivatives are used in combination with Nitrogen Tetroxide as an oxidizer. Typical values of Thrust and I_{sp} range from 400 N to 2500 N and 300 s to 350 s respectively
- **Chemical** propulsion based on **Non-Toxic** propellants: this class of system is currently under development with some applications already flight-proven. The range of propellant used is wide, while typical values of Thrust and I_{sp} are aligned with the Toxic option
- **Electric** propulsion: not as common as chemical propulsion, this class can guarantee high levels of I_{sp} from 1100 s to more than 2000 s, though with a significantly small level of Thrust, lower than 1 N. It's commonly used for orbital transfer applications rather than final orbit insertion

A valuable example, which served as starting point for this case study, is the Orbital Transfer Vehicle [1] developed by Rocket Factory Augsburg. Its data are reported in Table 1.1.

RFA OTV Data-sheet				
Dry Mass [kg]	Δv [m/s]	Max Thrust [kN]	$I_{sp,VAC}$ [s]	Propellant
250	2500	1.5	>300	Green

Table 1.1: RFA OTV specification

1.2 Green Propellant

Green propellants involve the use of different types of oxidizers and fuels with a reduced toxicity with respect to conventional propellant couples. The most used green propellants are [2]:

- Oxidizers: HTP 98%, HTP 87.5%, Nitrous Oxide
- Fuels: Methanol, Ethanol, Isopropanol, Ethane, Propane, Ethene, Propene, Ethyne, Propyne, Kerosene

In the case of the current project, the oxidizer is given as a requirement, being HTP 98%, but the green fuel is to be chosen.

1.2.1 Fuel Selection

In view of all the combinations of Hydrogen Peroxide and different fuels, it is necessary to perform a trade-off analysis between the possible fuel selections. To do so, six parameters of merit are chosen and weighed as follows:

- Toxicity: to weigh the fuels based on their toxicity level. The lower this parameter is, the better it is in terms of health. Inside this merit figure, many characteristics are included such as Toxicity Index, Vapor Hazard Ratio or GHS Acute Toxicity, among others [2]
- Storability: to differentiate the fuels according to their storability capabilities. To have a good propellant couple its storability characteristics have to be considered both in terms of safety and propulsion system size. Inside this category, parameters such as Vapor Pressure, Flammability or Stability are considered [2]
- Specific impulse: to weigh the fuels' performance. Specific impulse is one of the most important parameters in terms of performance that any engine has.
- Density: it is related to storability, but it is considered as a separate merit figure due to its importance inside these engines. The higher the density the lower the volume of the fuel and, therefore, the better for the engine design
- Combustion chamber temperature: to take into account the combustion process. It is strictly related to the heat inside the CC. The lower the temperature the less restrained the thermal requirements become
- Normal boiling temperature: to consider the cooling capability of the fuel. The higher it is the better for cooling the system

Table 1.2 shows all the data related to merit figures and the weights, on a scale from 1 to 5 [3], related to the different fuels considered [2].

To set the weights all the merit figures must be compared and balanced to determine their importance in the design. The heaviest parameter, with a value of 5, is the I_{sp} given it is the one related to the performance of the engine. Storability and ρ are both related to the system size and their weights are set to 3, due to their similarity and the aim of designing engines with reduced volume. Another intermediate figure is the T_b , a crucial factor for the cooling capability for the engine with a value of 3. The second to last heavy merit figure is T_{CC} , which is also related to thermal loads inside the combustion chamber. As thermal properties are already considered inside the boiling temperature, its weight is set to 2. Finally, toxicity's weight is set to 1.5 as all the included fuels are already acceptable in terms of this merit parameter.

Green Fuels Trade-Off						
Fuel	Toxicity [-]	Storability [-]	$\rho [kg/m^3]$	I_{sp} [s]	T_{CC} [K]	T_b [K]
Ethanol	14.0	6.0	0.789	312	2760	312
Isopropanol	13.5	5.5	0.784	314	2810	312
Propane	12.5	4.0	0.581	320	2850	312
Propene	12.5	4.0	0.611	322	2905	312
Propyne	12.5	3.5	0.692	312	3010	312
Ethane	12.5	3.5	0.499	322	2840	312
Ethene	12.0	4.0	0.567	325	2940	312
Ethyne	12.5	3.5	0.621	334	3110	312
Kerosene	12.5	6.0	0.800	316	2865	312
Weight [-]	1.5	3.0	3.0	5.0	2.0	3.0

Table 1.2: Trade-off values for green propellant fuels

With the mentioned values and weights, properly normalized and treated, Figure 1.1 is obtained. It can be appreciated that Kerosene is the option which better satisfies the merit parameters.

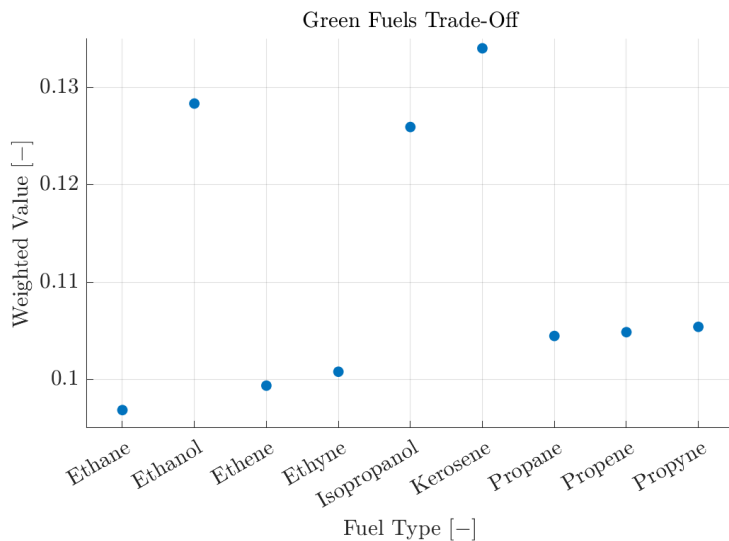


Figure 1.1: Green fuel trade-off

The chosen green propellant couple is Hydrogen Peroxide at 98% and RP-1 Kerosene.

1.2.2 Combustion Chamber Pressure Selection

Concerning the selection of the combustion chamber pressure, a literature review was performed selecting papers studying propulsion systems using HTP with a concentration higher than 90%. Due to the lack of available information, it was not possible to use only data linked to HTP with a concentration of 98%. From the different articles two main characteristics are considered: the thrust and the chamber pressure. There are many factors that influence the Thrust level, so a deeper analysis could be performed, but it goes outside the scope of this section.

Combustion Chamber Pressure vs Thrust			
HTP [%]	Thrust [N]	Pressure [bar]	Reference
90	1000	30	[4]
95	500	10	[5]
90	100	12.77	[6]
90	1200	30	[7]
90	100	28	[8]
90	330	9.5	[9]
96	200	10	[10]
90	40	12	[11]
90	2500	20	[12]
90	30	8	[13]
98	500	8	[14]
98	500	10.1	[15]
90	1112	32.75	[16]
98	6000	20	[17]

Table 1.3: Boundary types

The data is plotted in order to see better the trend. Considering Table 1.4, it is possible to see that, for this propellant couple and for Thrust levels under 1000 N the pressure of the combustion chamber is around 10 bar, while for Thrust levels > 1000 N the pressure goes from 12 bar to 30 bar. Therefore, it was selected a pressure of 20 bar for the nominal and doubled engines and a pressure of 10 bar for the halved green engine.

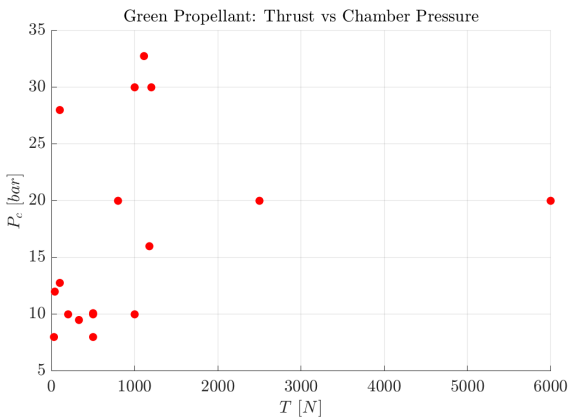


Table 1.4: Comparison of P_{CC} and T

1.3 Toxic Propellant

A second case with fixed hypergolic propellants is considered. The fuel used is part of the Hydrazine family, comprised by Hydrazine N_2H_4 , Monomethylhydrazine MMH and Unsymmetrical Dimethylhydrazine UDMH. On the other hand, Nitrogen Tetroxide N_2O_4 is used as an oxidizer. Pure form of this chemical is virtually never used due to the stress corrosion cracking. The inclusion of just 1-3% Nitric Acid NO inhibits this behaviour, without affecting the I_{sp} , and lowers the freezing point [18]. As such, a mixture of N_2O_4 and 1% NO is considered. However, due to this low concentration, the chemical analysis could be performed with N_2O_4 .

All three Hydrazine-based fuels can be used as monopropellants, though the higher I_{sp} given by its combination with N_2O_4 , makes them better suited for kick stage rockets and orbital maneuvering [19].

1.3.1 Combustion Chamber Pressure Selection

For the toxic couple, another literature review was carried out to identify comparable cases in order to fix the values of P_{CC} for the three different engines. To visualize a trend, the selected examples are linearly interpolated to then set P_{CC} with respect to the level of Thrust [20] [21].

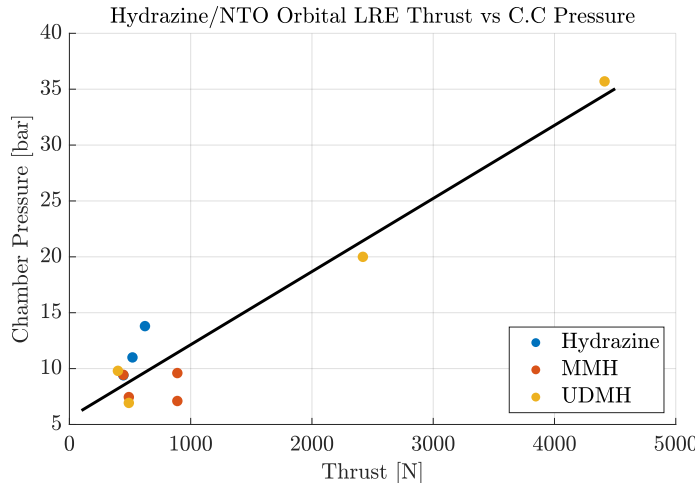


Figure 1.2: P_{CC} vs Thrust trend in orbital Hydrazine and NTO bipropellant engines

1.4 Materials and manufacturing

The selection of materials is constrained by different parameters depending on the considered component: tanks materials have to be compatible with pressurizing gas, oxidizer and fuel at storing conditions; while injection plate, combustion chamber and nozzle materials must be compatible with the mixture of fuel and oxidizer, and resist to high temperature and pressure conditions. In addition, the injection plate, combustion chamber and convergent part of the nozzle must be done in additive manufacturing.

1.4.1 Thrust chamber

A widely used material for Thrust chambers is Inconel 718: a nickel-chromium alloy with high strength and resistance to corrosion. It is commonly used in the aerospace industry, especially in propulsion systems [22][23][24][25], because of its ability to retain its mechanical properties at temperatures up to 800 K [26].

To reduce the temperature Inconel 718 reaches, a thermal barrier coating can be applied. For this purpose, the Yttria partly stabilized Zirconia (1.23) is selected, as it can withstand temperatures up to 1890 K [27]. The properties of this coating were retrieved using **Ansys Granta EduPack** [28].

Despite being listed as Class 2 under at 293.15 K [29] and Class 4 at 340 K, Inconel 718 was chosen due to its mechanical and thermal characteristics and its compatibility with AM techniques [30]. For missions with repeated use of the Thruster for long periods of time, such as those using it for periodic orbit maintenance, material selection should be re-evaluated for the injectors and other parts in long term contact with H_2O_2 .

1.4.2 Green Propellant Tanks

For the green propellant combination, it should be highlighted that Hydrogen Peroxide is incompatible with many common materials used for space propellant tanks, which may catalyze its decomposition into water and oxygen too early, posing an explosion risk [31]. Because of its high vapor pressure, H_2O_2 must be kept sealed in relatively heavy tanks [32]. Reference [29] offers a thorough material compatibility review of H_2O_2 . Several Aluminium alloys with Copper contents lower than 0.5%, such as Al 1060, Al 1160, Al 1260, Al 5254 and Al 5652,

show the best (Class 1) compatibility. Pure Aluminium can be coated onto the inside of a high strength Al alloy to create a compatible surface coating yet still retain the strength and hence lightness of the outer shell material. No stainless steel alloys show Class 1, but many achieve Class 2, which allows for repeated temporary exposure at 70 F. Cryogenic pre-strained 301 stainless steel has been successfully used in flight vehicles to store H₂O₂ [29]. Pure metals are rated as unsuitable (Class 4). Polytetrafluoroethylene (PTFE) coating makes SS and Ti-6Al-4V compatible with HTP [33].

Kerosene (RP-1) has few compatibility issues: most of the commonly used materials in space such as Aluminium, stainless steel, titanium, alloy steels, fiber-reinforced plastics can be used to build its tanks [34], with the only materials to be avoided being copper alloys [35]. An analysis was performed to calculate the weight of the tanks if made of Al 5254, SS 301 and Ti-6Al-4V. In the end, Ti-6Al-4V was chosen given its strength, which translates into a smaller weight. To simplify the analysis, the tanks for the fuel are the same material as the ones for the oxidizer. The final selection of materials is outlined in Table 1.5.

Material Selection	
Component	Material
RP-1 tanks	Ti 6Al-4V
H ₂ O ₂ tanks	Ti 6Al-4V
N ₂ tanks	Ti 6Al-4V
Piping	Al 5652
Thrust chamber	Inconel 718

Table 1.5: Material selection - Green case

1.4.3 Toxic Propellants Tanks

Compatible materials with MMH include certain stainless steels (303, 304, 321, or 347), Ti 6Al-4V, nickel, and Aluminium in general. But alloys containing molybdenum, iron, copper, and its alloys (such as brass or bronze), monel, magnesium, zinc, and some types of Aluminium alloys must be avoided [36]. It should be highlighted that the methyl group makes MMH less reactive than pure Hydrazine [37]. Therefore, materials compatible with N₂H₄ are as much or more compatible with MMH. Hydrazine tanks, pipes, injectors, catalysts, and valves are usually electrically heated to prevent freezing in cool ground weather or in outer space, and they must be cleaned and freed of all traces of impurities. Ti6Al-4V has one reference as not compatible for N₂H₄, though not for MMH [37].

Nitrogen Tetroxide is only mildly corrosive when pure but forms strong acids when moist or allowed to mix with water, readily absorbing moisture from the air. It can be stored indefinitely in sealed containers made of compatible materials. The moisture level of the NTO for this report is considered to be less than 0.1% or what is referenced as "green" or dry [38] [35]. Wet or "brown" NTO would rule out most metals except for 300 series Stainless Steels [35]. Pure Titanium is also only compatible with dry NTO, otherwise it is disadvantaged due to impact sensitivity when in contact with strong oxidizers. The Titanium alloy 6Al-4V is the only material compatible with NTO at temperatures near 400 K [38]. Materials compatible with both MMH and NTO include Al 7075, SS347, Ti 6Al-4V and Inconel, among others. For the same reasons as the green case, Ti 6Al-4V was chosen for the tanks and Inconel 718 for the thrust chamber. The final selection of materials is outlined in Table 1.6.

Material Selection	
Component	Material
MMH tanks	Ti 6Al-4V
NTO tanks	Ti 6Al-4V
N ₂ tanks	Ti 6Al-4V
Piping	Al 5652
Thrust chamber	Inconel 718

Table 1.6: Material selection - Toxic case

1.4.4 Additive Manufacturing

One of the requirements of the propulsion system described in this report is that injection plate and Thrust chamber have to be produced in additive manufacturing in a single block.

As previously stated, the chosen material for the Thrust chamber is Inconel 718 for both propellant couples. This material is ideal for additive manufacturing allowing for the production of complex shapes [39].

Considering the main characteristics of the engine designed in this report, an extensive research into the machinery available to produce AM components is done: Selective Laser Melting 800 3D printer [40], produced by SLM Solutions Group AG, is a feasible choice; its main productive characteristics and constraints are listed in Table 1.7.

Build Envelope [mm]	500 x 280 x 850
Minimum feature size [μm]	150
Variable layer thickness [μm]	20 - 90, more available on request
Maximum scan speed [m/s]	10
Real build rate [cm^3/h]	Up to 171

Table 1.7: SLM800 additive manufacturing 3D printer characteristics

SLM-built pieces have a buildup of internal stresses due to high cooling rates and newly melted layers contraction, and they also present anisotropy; those flaws can lead to cracks, deformations, micro-structure and mechanical properties local variations. For these reasons, as anticipated, post-processing is needed on additive manufactured pieces. The most used techniques for Inconel 718, summarized in Table 1.8, are stress relief, hot isostatic press, solutionized and aging to reduce porosity and defects, surface finishing to reduce roughness [41].

Post-processing method	Technical data for Inconel 718
Stress relief	30 min at 1255 K or 90 min at 1338 K
HIP	4 h at 1393 K and 200 MPa
Solutionize	1 h at 1253 K
Aging	8 h at 993 K or Cooling at 893 K or Kept at 893 K for 18 h

Table 1.8: Inconel 718 post-processing techniques

Regarding the final piece, SLM can reach a minimum roughness of 17-20 μm , and holes shall have a diameter larger than 0.5 mm [42].

Chapter 2

Engines Modelling

Nozzle and combustion chamber design is carried out following an iterative process described in the flowchart reported below:

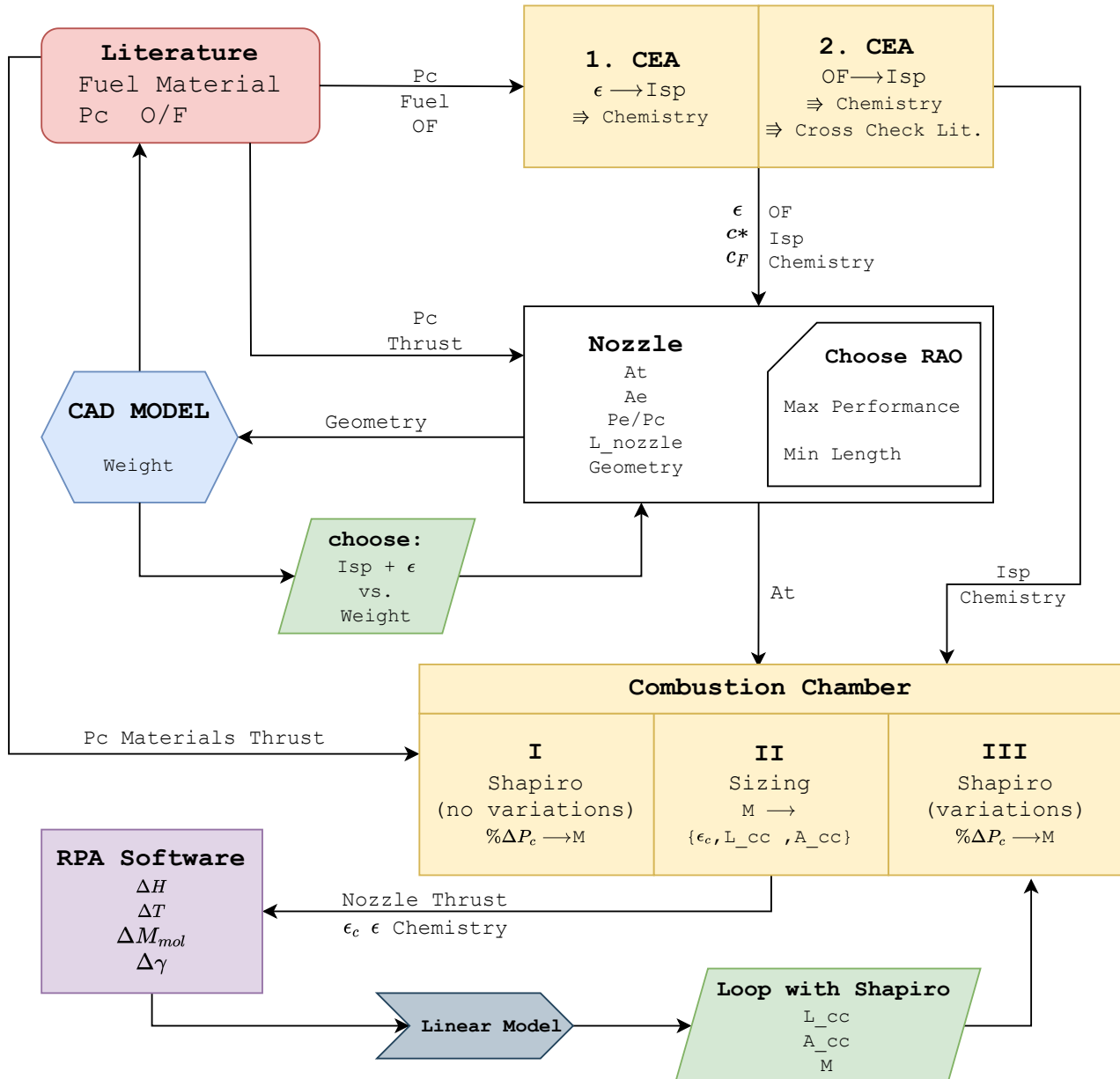


Figure 2.1: Workflow followed for iterative design of Nozzle and Combustion Chamber

2.1 Nozzle Design

The nozzle design process is focused on obtaining optimal system parameters in terms of performance, dimensions, and mass. The work has been divided into three major steps:

- First, a NASA CEAM analysis is performed to fix the $\frac{O}{F}$ and retrieve a set of parameters at various expansion ratios ϵ
- Then, a 15 deg conic nozzle is designed using isentropic relations and some performance values such as the thrust coefficient. This conic nozzle is later used to proceed with the Rao approximation and to retrieve the parameters of a bell nozzle
- Lastly, an optimization process is performed to select ϵ to maximize the Vacuum Specific Impulse as well as minimize the nozzle mass

A description of the design workflow is given in the following sections, while the results for all six engines are shown in Section 2.2.

2.1.1 CEAM Analysis

The NASA CEAM is iteratively used to retrieve the optimal parameters to be fed to the nozzle and combustion chamber design. The analysis is performed by setting $\frac{O}{F}$ and ϵ as variables, while the $I_{sp,VAC}$ as the performance index. The inputs of the problem are:

- Pressure Chamber - P_{CC} : obtained from Subsections 1.2.2 and 1.3.1 for the green and toxic case respectively
- Reactants: chemical composition and storage temperature

The values are reported in Table 2.1

NASA CEAM Input Parameters						
	Green			Toxic		
	Halved	Nominal	Doubled	Halved	Nominal	Doubled
P_{CC} [bar]	10.0	20.0	20.0	8.5	12.5	18.0
Oxidizer [298.15 K]	H_2O_2 (98%) + H_2O (2%)			N_2O_4		
Fuel [298.15 K]	RP-1			$CH_6N_2(L)$		

Table 2.1: Trade-off values for green propellant fuels

The study is implemented using the Rocket Problem, while, for the reacting flow model, Bray is chosen over Shifting Equilibrium and Frozen since it gives more accurate results. A comparison between the three of them is given in Appendix C.

The iterative process is described in the following sections, while the final results are reported in Table 2.2.

2.1.1.1 Multi-variable Optimization

As the first step, a multi-variable optimization is performed to identify the optimal ranges of $\frac{O}{F}$ and ϵ . This analysis is performed on the nominal engines in both green and toxic configurations.

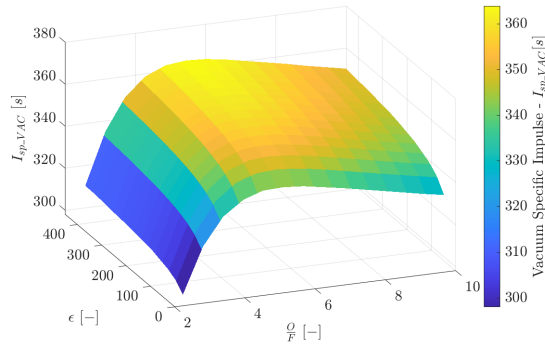


Figure 2.2: Green couple - $\frac{O}{F}$ and ϵ trade-off

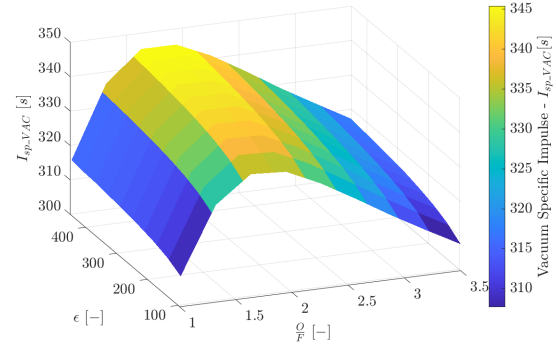


Figure 2.3: Toxic couple - $\frac{O}{F}$ and ϵ trade-off

For both cases, as expected, the $I_{sp,VAC}$ shows a peak with respect to the $\frac{O}{F}$ at its stoichiometric condition. Instead, a settled increasing behaviour can be seen in $I_{sp,VAC}$ as ϵ gets higher.

One of the two variables needs to be fixed to proceed with the analysis. As shown above, the optimal ranges of $\frac{O}{F}$ are restricted and coincide with the ones found in the literature. Therefore, the following values are set:

- Green reactants: $\frac{O}{F} = 6.17$
- Toxic reactants: $\frac{O}{F} = 1.6$

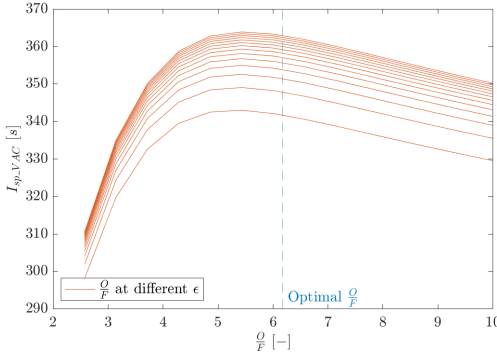


Figure 2.4: Green couple - $I_{sp,VAC}$ at different ϵ

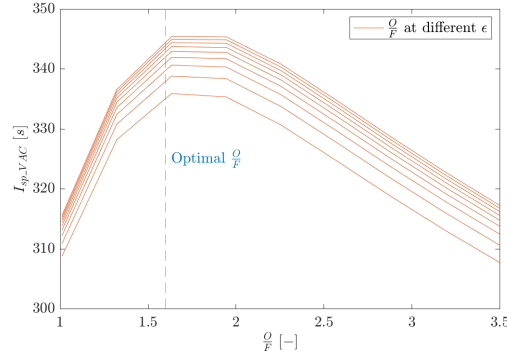


Figure 2.5: Toxic couple - $I_{sp,VAC}$ at different ϵ

The choice of the optimal value of $\frac{O}{F}$, illustrated in 2.4 and 2.5), is the result of a cross-check between the data given by CEAM and the data found in the literature. For the toxic case, CEAM's $\frac{O}{F}$ that grants the best performance matches the one found in the literature. However, in the green case, a discrepancy can be seen; specifically, the CEAM gives an $\frac{O}{F}$ slightly lower than the one reported in the literature [2].

2.1.2 Expansion Ratio Optimization

To select the optimal expansion ratio for all cases, the first step is to design the nozzle geometry. Starting from a conical shape, the Rao is retrieved and iteratively solved at various ϵ .

2.1.3 Conic Nozzle

2.1.3.1 Divergent Section

Given ϵ and the heat-specific ratio γ , the chamber and exit pressure ratio $\frac{P_e}{P_{CC}}$ is computed from Equation 2.1

$$\frac{1}{\epsilon} = \frac{A_t}{A_e} = \left(\frac{\gamma + 1}{2} \right)^{\frac{1}{\gamma-1}} \left(\frac{P_e}{P_{CC}} \right)^{\frac{1}{\gamma}} \sqrt{\frac{\gamma + 1}{\gamma - 1} \left[1 - \left(\frac{P_e}{P_{CC}} \right)^{\frac{\gamma-1}{\gamma}} \right]} \quad (2.1)$$

This pressure ratio is used to retrieve the thrust coefficient C_F using the Equation 2.2, in which the ambient pressure is set to zero as the mission takes place in space.

$$C_F = \sqrt{\frac{2\gamma^2}{\gamma-1} \left(\frac{2}{\gamma-1} \right)^{\frac{\gamma+1}{\gamma-1}} \left[1 - \left(\frac{P_e}{P_{CC}} \right)^{\frac{\gamma-1}{\gamma}} \right] + \frac{P_e}{P_{CC}} \cdot \epsilon} = \frac{T}{P_c A_t} \quad (2.2)$$

Through the throat area A_t is then retrieved from the same expression, and from Equation 2.1 the exit area is also calculated. Then, the diameters of both the throat and exit sections can be computed. Once these key parameters are obtained, the length and efficiency of the nozzle are estimated. To do so, the divergent angle $\alpha = 15$ deg is used in Equations 2.3 and 2.4.

$$\lambda_{conic} = \frac{1 + \cos \alpha}{1} \quad (2.3)$$

$$L_{div-conic} = \frac{D_e - D_t}{2 \tan \alpha} \quad (2.4)$$

Finally, in order to obtain the desired thrust, the 2D losses must be taken into account. The necessary one-dimensional thrust must be retrieved through the efficiency of the nozzle and Equation 2.5.

$$T_{1D-conic} = \frac{T_{desired}}{\lambda_{conic}} \quad (2.5)$$

2.1.3.2 Convergent Section

From literature [43], the convergent angle is set to a value of $\beta = 45$ deg, and using the procedure in Chapter 2.2, the combustion chamber diameter D_{CC} is obtained. Inputting these two values in Equation 2.6, the convergent section length is computed.

$$L_{con-conic} = \frac{D_{CC} - D_t}{2 \tan \beta} \quad (2.6)$$

2.1.4 Rao Approximation

Once obtained the conic nozzle, the Rao approach is applied [44] using the graphs in Section B.1. There are multiple ways to proceed. For this case study two different approaches are evaluated:

- Minimum Length Approach: the length is reduced to its minimum compared with the reference conic nozzle assuming more losses
- Maximum Performance Approach: the performance is optimized by having the maximum possible length

2.1.4.1 Minimum Length Approach

In this approach, the length of the equivalent 15 deg conic nozzle is reduced to 60% of its original value. Therefore:

$$L_{Rao-ML} = 0.6 \cdot L_{div-conic}$$

Then, the initial and final parabola angles are retrieved using the graphs in Section B.1. Since all the ϵ are greater than 50 and the graphs have a clear asymptotic behavior, $\theta_{i-ML} = 48$ deg and $\theta_{e-ML} = 13.5$ deg. Finally, the new nozzle efficiency is computed using Equation 2.7, obtaining the new α by inverting Equation 2.4.

$$\lambda_{Rao} = \frac{1 + \cos\left(\frac{\alpha+\theta_e}{2}\right)}{2} \quad (2.7)$$

2.1.4.2 Maximum Performance Approach

The same workflow of the minimum length approach is applied to retrieve the maximum performance bell nozzle by setting:

$$L_{Rao-MP} = L_{div-conic}$$

In this method, $\theta_{i-MP} = 39$ deg and $\theta_{e-MP} = 4.5$ deg. Finally, the new α is obtained by inverting Equation 2.4 and the efficiency is computed through Equation 2.7.

2.1.5 Optimization & Results

Fixing the oxidizer to fuel ratio, a one-variable optimization is performed. A set of possible ϵ is first fed to the CEAM to compute the relative $I_{sp,VAC}$ and γ . The values are used to retrieve a set of geometries assuming maximum performance. A trade-off analysis is performed by comparing the increase in $I_{sp,VAC}$ granted by higher ϵ with respect to the relative increase in mass, given as the sum of nozzle and fuel.

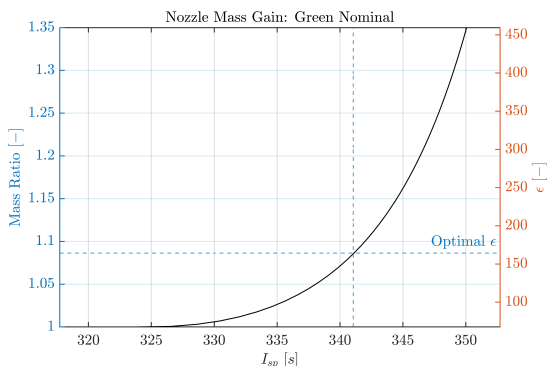


Figure 2.6: Green couple - mass gain at different ϵ

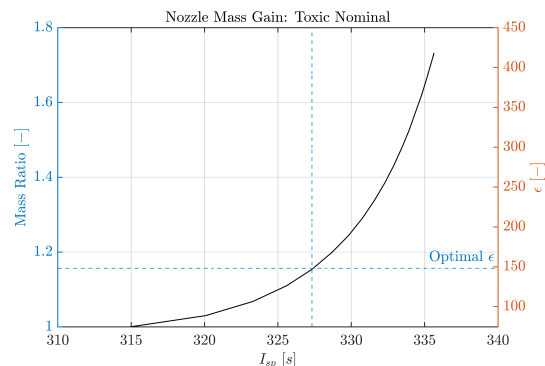


Figure 2.7: Toxic couple - mass gain at different ϵ

Figure 2.6 and 2.7 show the output of the process in the nominal case for the green and toxic configuration, respectively. The final values of ϵ , reported in Table 2.2, are obtained by looking at the point in which the marginal return in $I_{sp,VAC}$ becomes smaller with respect to the mass increase.

	Nozzle Results					
	Green halved	Green nominal	Green doubled	Toxic halved	Toxic nominal	Toxic doubled
$\epsilon [-]$	172	164	162	164	148	180
$r_t [m]$	0.0084	0.0084	0.0119	0.0093	0.0109	0.0129
$\frac{P_e}{P_{CC}} [-]$	0.0007	0.0007	0.0007	0.0006	0.0006	0.0005
$L_{Rao-MP} [m]$	0.3788	0.3707	0.5210	0.4110	0.4558	0.5969
$L_{Rao-ML} [m]$	0.2273	0.2224	0.3126	0.2466	0.2735	0.3581
$\lambda_{Rao-MP} [-]$	0.9928	0.9928	0.9928	0.9928	0.9928	0.9928
$\lambda_{Rao-ML} [-]$	0.9734	0.9734	0.9734	0.9734	0.9734	0.9734

Table 2.2: Nozzle results for the six different cases

Maximum performance nozzle is selected, as performance is weighted to be more important than the total size in the analysis. It can be noticed that applying the minimum length approach the length difference is between 10 and 20 cm for all six engines, which would translate into a significant reduction in weight. Nevertheless, since the nozzle is one of the lightest elements inside the engine, an extra amount of performance is prioritised in the design.

2.2 Combustion Chamber Model

An iterative approach is implemented to find the optimal combustion chamber dimensions. Two main constraints are considered: Mach number at the end of the combustion chamber must be smaller than 0.6 and the total pressure loss shall not exceed 0.5%.

The geometry is retrieved when inputting the nozzle throat area and the propellant characteristics from **CEAM** into a **Matlab** code. This script combines the Shapiro model, the formulas for the characteristic length, and the variations between inlet and outlet conditions calculated with the **RPA software**.

The process is divided into three steps, which will be explained in detail in the following sections. These are looped and repeated several times until a suitable solution is found:

- Implementation of the Shapiro model, using several Mach numbers to compute the pressure losses
- Usage of the characteristic length to calculate the length and area of the combustion chamber
- Inputting of the data in the **RPA software** to obtain the variation of some of the independent variables later used in the Shapiro model

2.2.1 Shapiro model

The Shapiro model is solved numerically in the **Matlab** code. The variation of the independent variables are considered as:

- dA : considered as zero since the combustion chamber is cylindrical
- dQ : the variation of heat is calculated using the following equation $dQ = c_p \cdot T \cdot dm$, where $dm = \rho \cdot A \cdot dx$
- dW : variation of work is considered equal to zero since there are no moving parts inside the chamber

- dH : the variation of enthalpy is considered linear with initial and final values obtained with RPA software
- $dDrag$: due to the nature of the combustion chamber, no drag forces are considered
- $d\dot{m}$: since there is no extra mass entering the combustion chamber, other than from the injectors, this value can be taken as zero
- dM_{mol} : the variation of molar mass is considered linear with initial and final values obtained with RPA software
- $d\gamma$: the variation of specific heat ratio is considered linear with initial and final values obtained with RPA software

On the first iteration, all these values are set to zero, in order to have a first approximation of the losses. After the first loop, already having some initial values of the geometry, these values are set to be equal to the ones found from the RPA software. In the next graph it is possible to see how the pressure losses increase with the Mach number. For continuing the iteration process, a Mach number is chosen in order to have losses inferior to 0.5%.

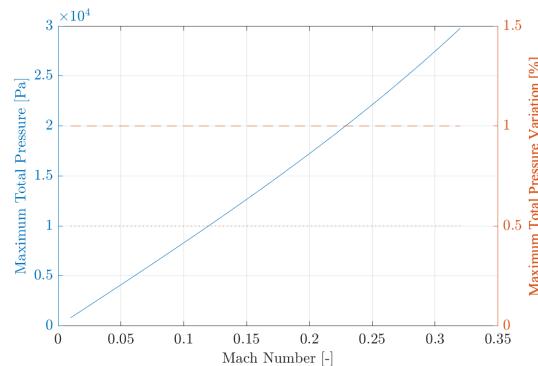


Figure 2.8: Green couple - M optimization

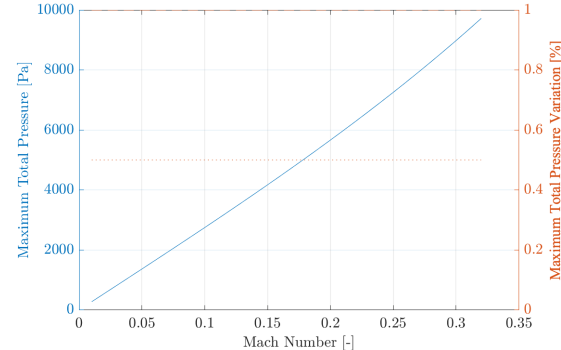


Figure 2.9: Toxic couple - M optimization

2.2.2 Selection of contraction ratio

From the following equations, the Mach number and length of the combustion chamber are computed as a function of ϵ_c :

$$L_{CC} = \frac{L^* \cdot A_t}{\epsilon_c \cdot A_t} = \frac{V_{CC}}{A_{CC}} \quad (2.8)$$

$$M_{CC} = \frac{\dot{m}_p}{\rho \cdot \epsilon_c \cdot A_t} \cdot \frac{1}{a} = \frac{v_{gasCC}}{a} \quad (2.9)$$

Selecting a Mach number equal or inferior to the one found in the previous section, it is possible to obtain L_{CC} and ϵ_c .

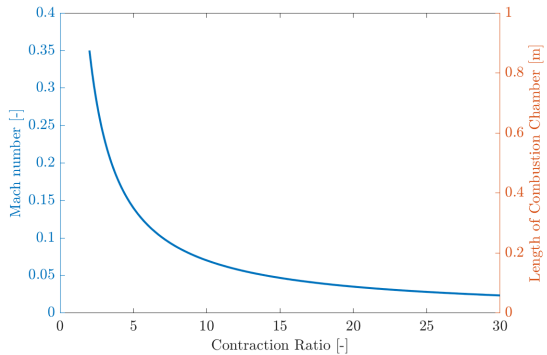


Figure 2.10: Green couple - ϵ_c , M_{CC} and L_{CC} trade-off

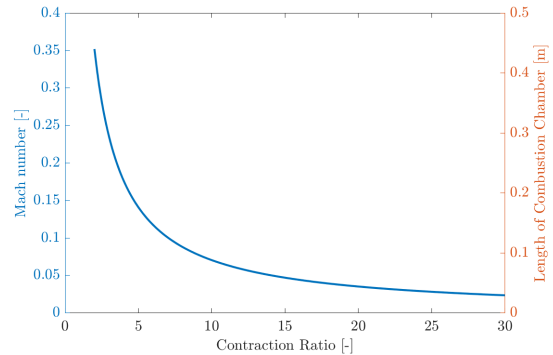


Figure 2.11: Toxic couple - ϵ_c , M_{CC} and L_{CC} trade-off

2.2.3 Results

The outputs of the combustion chamber modelling are reported in the following Table 2.3:

Combustion Chamber Results						
	Green halved	Green nominal	Green doubled	Toxic halved	Toxic nominal	Toxic doubled
ϵ_c [-]	7.3	5.4	3.8	5.1	4.7	3.4
M_{CC} [-]	0.1	0.129	0.19	0.14	0.15	0.205
L_{CC} [m]	0.2671	0.3610	0.5131	0.1614	0.1751	0.2420
A_{CC} [m^2]	0.0016	0.0012	0.0017	0.0014	0.0018	0.0018

Table 2.3: Combustion chamber results for the six different cases

These values are then inputted into RPA software, in order to obtain the thermodynamic characteristics of the flow.

2.3 Injectors

2.3.1 MMH-NTO injectors

The selected type of injectors for the toxic propellant couple is an unlike doublet, chosen based on the $\frac{Q}{F}$. These type of injectors are common for Earth storable bipropellants [45] and widely used for the MMH NTO combination [46]. The fuel injector has a discharge coefficient $C_D = 0.7$ and a diameter based on the most limiting additive manufacturing capabilities, further explained in Subsection 1.4.4. The injectors are inclined to cancel the tangential momentum and the sum of the angles was kept within the ranges recommended in [46]. Finally, the injection velocities are calculated. The pressure drop is tuned to ensure velocities are higher than 20 m/s. For the halved case, since the chamber pressure is smaller, the injection velocity is greatly reduced compromising the atomization. This shows one of the difficulties of miniaturising systems: the smaller pressure drops available demand for higher efficiencies in the injector. The results are outlined in Subsection 2.3.3.

2.3.2 H2O2-RP1 injectors

The selected type of injectors for the green propellant couple is a triplet, chosen based on the larger $\frac{Q}{F}$. The fuel injector diameter is again chosen based on the most limiting additive

manufacturing capabilities and with an initial $C_D = 0.7$. Finally, the injection velocities are computed and the pressure drop is tuned to ensure velocities are higher than 20 m/s. The same behaviour as for the toxic case is observed: the miniaturised system requires a more efficient discharge to guarantee the atomization of the oxidizer. In this case, the C_D was assumed to be 0.9 for this case. This would require extensive testing and possibly post processing of the plate, which might not be possible for this design. The results are outlined in Subsection 2.3.3.

2.3.3 Results

Injector Specifications - Toxic Case					
Thrust	Propellant	D [mm]	C_D [-]	v_{inj} [m/s]	ΔP [%]
Halved	MMH	0.50	0.7	19.57	$0.4 \times P_{CC}$
	NTO	0.52	0.8	17.34	
Nominal	MMH	0.50	0.7	23.73	$0.4 \times P_{CC}$
	NTO	0.52	0.8	21.03	
Large	MMH	0.50	0.7	24.66	$0.3 \times P_{CC}$
	NTO	0.52	0.8	21.86	

Table 2.4: Injector properties for the toxic couple

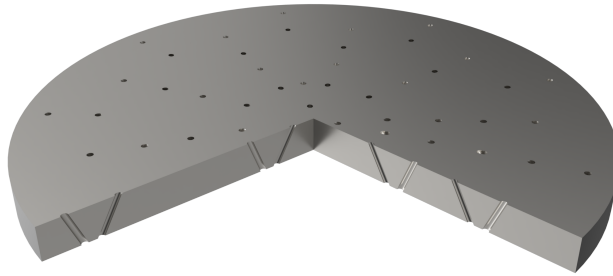


Figure 2.12: Toxic couple injection plate

Injector Specifications - Green Case					
Thrust	Propellant	D [mm]	C_D [-]	v_{inj} [m/s]	ΔP [%]
Halved	RP1	0.50	0.7	20.58	$0.4 \times P_{CC}$
	H ₂ O ₂	0.64	0.9	19.90	
Nominal	RP1	0.50	0.7	26.94	$0.4 \times P_{CC}$
	H ₂ O ₂	0.70	0.8	23.17	
Large	RP1	0.50	0.7	26.94	$0.3 \times P_{CC}$
	H ₂ O ₂	0.70	0.8	23.17	

Table 2.5: Injector properties for the green couple

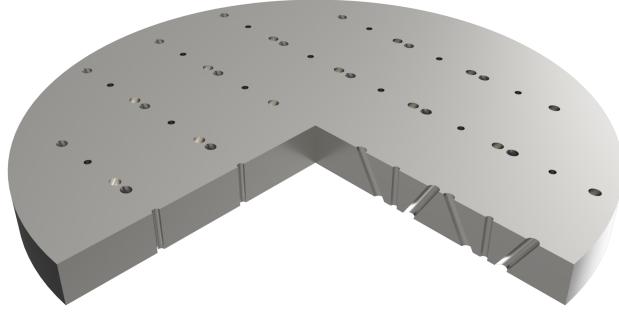


Figure 2.13: Green couple injection plate

2.4 Pressurization System

2.4.1 Pressure Losses

The bipropellant feeding system is composed of fuel and oxidizer tanks each of which is connected to an individual pressurizer tank. The selected pressurant gas is N₂, compatible with both toxic and green couples and with many materials commonly used for tanks in space [47]. The material chosen for all the tanks is Ti-6Al-4V [48], an optimal combination of yield strength and density, and its compatibility with both the toxic and the green propellant couple [36]. Particular attention has to be paid to H₂O₂ since its high concentration requires an additional coating of Polytetrafluoroethylene (PTFE) on the internal walls [48]. The four tanks are positioned at the same level on a common structure in a configuration that allows to balance the mass distribution, as shown in Figure 1 and Figure 2. A pressure cascade analysis is performed in order to size the volume and mass of the propellant and pressurizer tanks starting from the combustion chamber pressure and considering pressure drop contributes from injector plate, feeding lines, valves, and dynamic flow.

$$P_{p,tank} = P_{CC} + \Delta P_{injector} + \Delta P_{feeding} + \Delta P_{valve} + \Delta P_{dynamics} \quad (2.10)$$

The valves for the pressurizer and propellant tanks are latch valves from Moog [49], that guarantee high MEOP and no power consumption to maintain the open and close position. The pipelines are designed of diameter $D_{pipe} = 1$ cm and length $L_{pipe} = 1.1$ m to guarantee the required pressure drop at the injector [50] described in Subsection 2.3.3.

In the case of the H₂O₂, an additional pressure drop due to catalytic bed is considered, in which a bed length of $L_{cat} = 5$ cm is chosen to obtain a complete dissociation of H₂O₂. The associated pressure drop is computed from Ergun model.

$$\Delta P_{bed} = 150 \cdot L_{cat} \cdot \mu \cdot \frac{(1 - \epsilon_p)^2}{\epsilon_p^3 \cdot D_{cat}^2} \cdot u_p + 1.75 \cdot L_{cat} \cdot \mu \cdot \frac{1 - \epsilon_p}{\epsilon_p^3 \cdot D_{cat}} \cdot u_p^2 \quad (2.11)$$

With porosity $\epsilon_p = 0.4$ and catalyst granular size $D_{cat} = 1.4$ mm as described in [51]. The results of pressure cascade analysis are reported in Fig.2.14 and in the Appendix D. To obtain the velocity needed for the atomization at the exit of the injection plate, a $\Delta P_{required}$ for each couple has to be reached with a proper design of the propulsion system. The pressure drops coming from the pressure cascade analysis in Table 2.6, defined as difference between propellant tank pressure and chamber pressure, reach in all 6 considered case the required value.

	Pressure cascade Results					
	Green halved	Green nominal	Green doubled	Toxic halved	Toxic nominal	Toxic doubled
P_{cc} [bar]	10.0	20.0	20.0	8.5	12.5	18.0
$\Delta P_{required}$ [bar]	3.00	8.00	8.00	2.55	5.00	7.20
$\Delta P_{fuel,model}$ [bar]	6.210	8.210	6.210	6.170	6.970	8.074
$\Delta P_{ox,model}$ [bar]	9.24	11.24	11.24	8.68	9.48	10.58

Table 2.6: Pressure cascade results

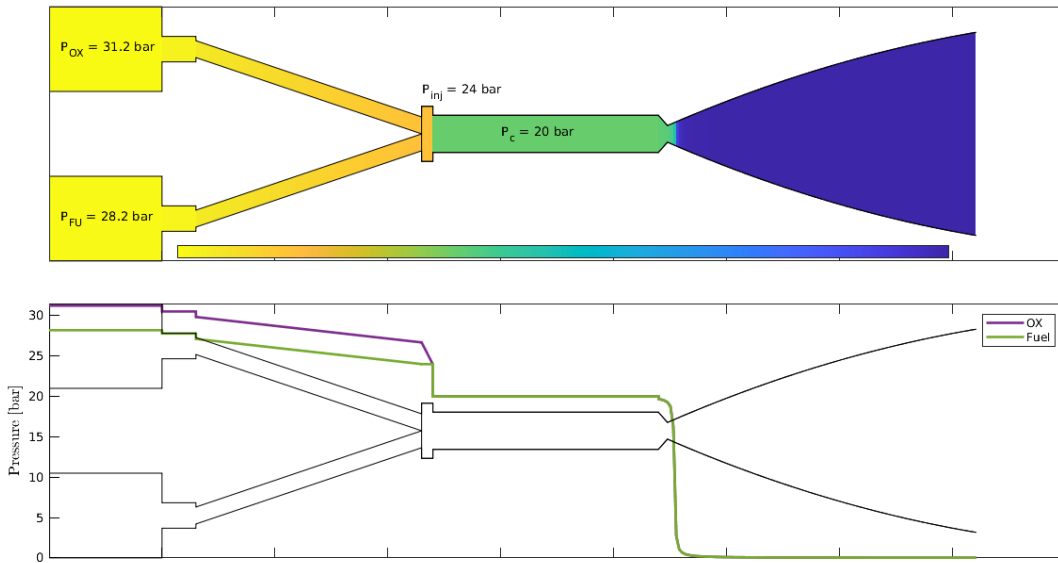


Figure 2.14: Pressure cascade - Green nominal. Starting from the tank pressure of the propellant, the pressure jumps correspond respectively to $\Delta P_{dynamics}$, ΔP_{valve} , $\Delta P_{feeding}$, ΔP_{bed} only for H_2O_2 and $\Delta P_{injector}$.

The volumes of fuel and oxidizer tanks are obtained from the burning time t_b and volumetric flow rate \dot{V}_p , computed using mission specification data. These results are increased by a 5% margin to take into account unexpected behaviour, such as propellant trapped in the pipes, and an additional 2% margin to consider volume change of the propellants. Regarding the pressurizer volume sizing, the amount of N_2 is computed considering an initial temperature of 298.15 K and a final temperature of 5 K above the freezing point of propellants in the green and toxic couples.

	Volume Sizing Results					
	Green halved	Green nominal	Green doubled	Toxic halved	Toxic nominal	Toxic doubled
$V_{fuel,tank}$ [m^3]	0.053	0.052	0.052	0.140	0.140	0.140
$V_{ox,tank}$ [m^3]	0.18	0.18	0.18	0.13	0.13	0.13
$V_{press,fuel,tank}$ [m^3]	0.042	0.041	0.041	0.140	0.140	0.140
$V_{press,ox,tank}$ [m^3]	0.13	0.11	0.11	0.13	0.12	0.11
V_{tot} [m^3]	0.405	0.383	0.383	0.540	0.530	0.520

Table 2.7: Volume sizing results

The toxic couple has a higher total volume with respect to the green couple. It was also found that, for the green propellants, there's a difference in the size between oxidizer and fuel tanks, that could create additional disturbance torque [52].

Regarding sizing of propellant and pressurizer tanks, a spherical structures was considered, with a wall thickness capable of holding twice the nominal pressure P_{fluid} computed in Equation 2.10 for the corresponding fluid.

$$t = 2P_{fluid} \frac{r_{press,fluid,tank}}{2\sigma_{yield}}; \quad (2.12)$$

where $r_{press,fluid,tank}$ is the pressurizer tank radius and σ_{yield} is the yield strength of the Ti-6Al-4V.

Mass Sizing Results						
	Green halved	Green nominal	Green doubled	Toxic halved	Toxic nominal	Toxic doubled
m_{fuel} [kg]	41.75	40.88	40.88	119.19	119.19	117.60
m_{ox} [kg]	257.59	252.21	252.21	190.70	190.70	188.21
$m_{fuel,tank}$ [kg]	1.29	2.19	2.19	3.09	4.11	5.42
$m_{ox,tank}$ [kg]	5.33	8.48	8.48	3.49	4.46	5.72
$m_{p,tot}$ [kg]	305.96	303.76	303.76	317.07	318.46	316.95
$m_{press,fuel}$ [kg]	2.390	4.077	4.077	6.110	8.110	10.710
$m_{press,ox}$ [kg]	7.20	10.95	10.95	5.76	7.12	8.90
$m_{press,fuel,tank}$ [kg]	3.19	5.44	5.44	8.16	10.83	14.31
$m_{press,ox,tank}$ [kg]	9.62	14.63	14.63	7.70	9.51	11.89
$m_{press,tot}$ [kg]	22.400	35.097	35.097	27.730	35.570	45.810
m_{dry} [kg]	19.43	30.74	30.74	22.44	28.85	37.34
m_{tot} [kg]	328.36	338.86	338.86	344.80	354.03	362.76

Table 2.8: Mass sizing results

Table 2.8 shows lower values for both total mass of the propellant mass system $m_{p,tot}$ and of the pressurizer mass system $m_{press,tot}$ (fluid + tank mass) for the green couple. The sum of the mass of all the tanks in the 6 cases studied never exceeds m_{dry} 40 kg.

Chapter 3

Thermal Analysis

Thermal analysis is split into two different steps:

- First, a thermal analysis is performed with **RPA software**. Regenerative cooling is applied to get the wall temperature down to 800 K, the operational temperature of Inconel 718[39]
- Secondly, in case the mass flow rate of the fuel is not enough, a coating is applied. Its thickness is calculated to guarantee the survivability of the engine

This process is followed for all six engines. For the set of toxic engines, even though the oxidizer mass flow rate is larger, the fuel is picked as coolant due to its bigger saturation temperature [53]. In the case of the green propellant, Hydrogen Peroxide is the one selected for regenerative cooling. The main problem with this choice is the possibility of an exothermic decomposition reaction. For this reason, a conservative saturation temperature of 100 K is chosen for all three engines [54].

3.1 Regenerative Cooling Thermal Analysis

To have a more precise analysis, **RPA software** is used to retrieve all the thermodynamic data without applying any cooling. The wall temperature and heat flux evolution are obtained by setting all the options to match the exact conditions of the case. Then, the model of the engine is discretised in small portions assuming cylindrical areas.

The local heat flux is multiplied by its associated area to compute the total heat, which has to be matched by the heat coming from the coolant. Therefore, the increment of coolant temperature is estimated through Equation 3.1 [44].

$$Q_{hot-gas} = Q_{coolant} = C_{pc} \cdot \dot{m}_{coolant} \cdot \Delta T_{coolant} \quad (3.1)$$

The $\Delta T_{coolant}$ is used then to calculate the final temperature of the fuel. Finally, it is compared with the saturation temperature to ensure that it does not exceed it. If the regenerative cooling strategy is not enough, then a coating must be applied.

3.2 Coating Design and Validation

To design the one-layer coating, the thermal-electrical analogy and Fourier's equations are used to create a model [44] [55] [56]. This method can be used since steady state is assumed. For the thermal barrier coating, the implemented material is, as mentioned in Subsection 1.4.1, Yttria partly stabilized Zirconia (1.23).

The coating thickness is obtained through an iterative process explained below. Since the sections are discretised as cylinders, both the coating and the walls can be modeled as cylindrical thermal resistances, calculated with Equation 3.2.

$$R_{cyl} = \frac{\ln \frac{r_e}{r_i}}{2\pi \cdot k \cdot L_{cyl}} \quad (3.2)$$

Knowing the heat coming from the hot gases, the ΔT of the coating and the temperature of the wall are calculated through Equation 3.3. This is a worst case scenario approach, since the

coating is considered to be at the same temperature of the gases. Therefore, it overestimates the internal temperature of the thermal barrier.

$$\Delta T_{coat} = T_{hot-gas} - T_{ext-coat} = Q_{hot-gas} R_{cyl-coat} \quad (3.3)$$

The coating thickness is then stored if $T_{ext-coat}$, the temperature of the wall, is less than 800 K. Finally, the temperature of the thermal barrier must be retrieved to check that the coating will survive the combustion process. In order to do so, the Fourier Equation 3.4 is applied, assuming that the coolant starts with a temperature of 273.15 K (storage temperature of the liquid) at the beginning of the combustion chamber, and setting its maximum temperature equal to the boiling temperature.

$$q = -k \cdot \frac{\Delta T}{\Delta x} \quad (3.4)$$

3.3 Results Discussion

The coating design and cooling system present several challenges for the different engines.

Regenerative Cooling Results						
	Green halved	Green nominal	Green doubled	Toxic halved	Toxic nominal	Toxic doubled
ΔT [K]	181.4	145.5	144.5	205.7	165.9	151.8
T_{final} [K]	454.6	419.0	417.6	478.7	438.9	424.8
T_{sat} [K]	373.15	373.15	373.15	450.00	461.00	488.00
$\dot{m}_{coolant}$ [kg/s]	0.129	0.257	0.515	0.060	0.120	0.238

Table 3.1: Regenerative cooling results for the six different cases

On Table 3.1 are presented the results obtained by applying the cooling system. It is possible to appreciate that for the toxic nominal and toxic doubled, the application of a coating is not necessary. It should be taken into consideration that these results are idealistic and if a cooling jacket was to be designed the boiling temperature could be lower due to higher pressure drops.

In the graphs shown below it is possible to see that the throat area exhibits an increase in the temperature of the coating. This behaviour is expected, since the throat area presents an increase in both heat flux and adiabatic flame temperature. This causes a high temperature zone where the selected coating would achieve non survivable temperatures higher than 1890 K. It is important to remark that the wall temperature remains at a constant temperature close to 800 K not shown in the figures bellow.

Beware that for the cases where the coating is applied the cooling system is considered as covering from the combustion chamber to the convergent part of the nozzle. It was found that the coating is more than enough to ensure the survivability of the wall on the divergent part of the nozzle.

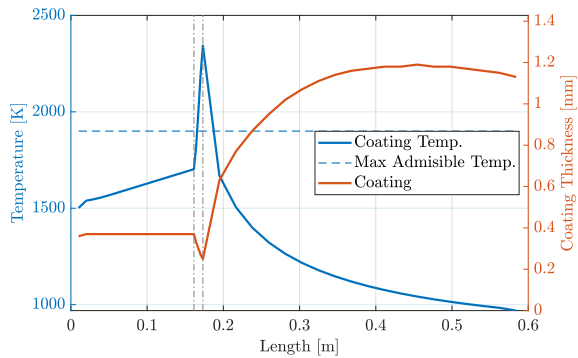


Figure 3.1: Coat temperature and thickness - Toxic halved

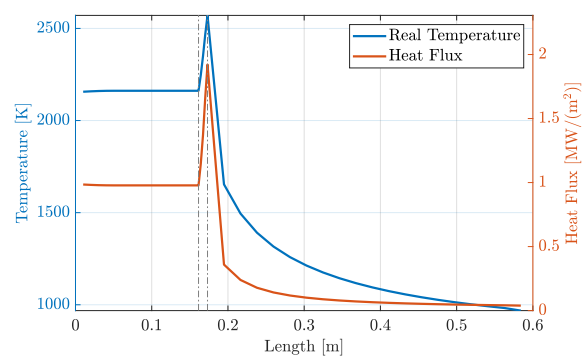


Figure 3.2: Wall temperature and heat flux - Toxic halved

As seen above in Figures 3.5 and 3.6, the toxic halved case is the one that performs better with the designed cooling system and coating. These results can be expected since this engine presents a lower heat flux and has the lowest convective heat coefficient of them all.

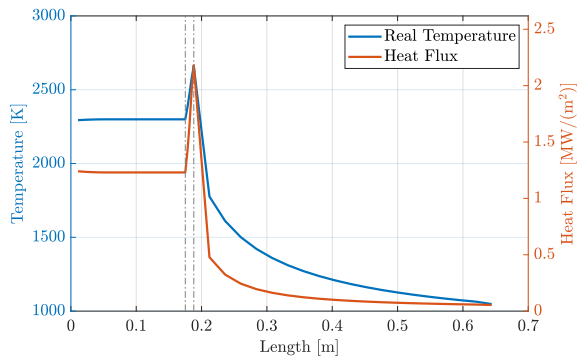


Figure 3.3: Wall temperature and heat flux - Toxic nominal

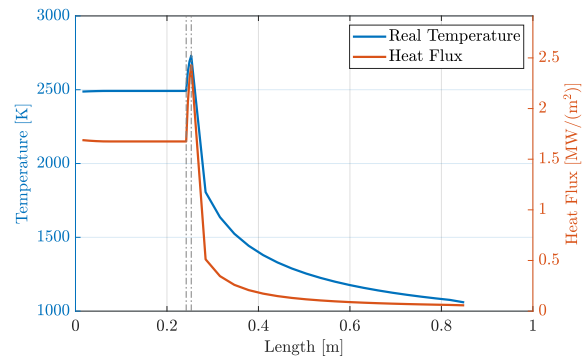


Figure 3.4: Wall temperature and heat flux - Toxic doubled

The graph is not reported here since it was found that a coating was not necessary for the protection of the walls. Above are presented the adiabatic flame temperature and the total heat flux of the toxic nominal and the toxic doubled engines, Figures 3.3 and 3.4.

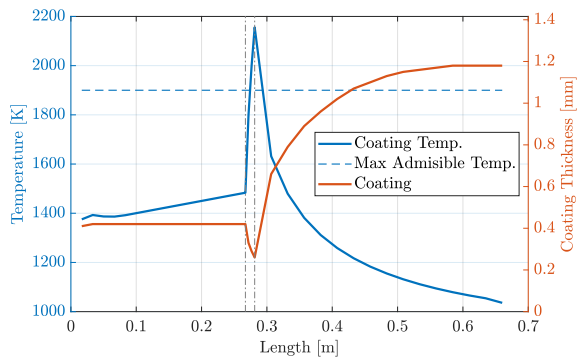


Figure 3.5: Coat temperature and thickness - Green halved

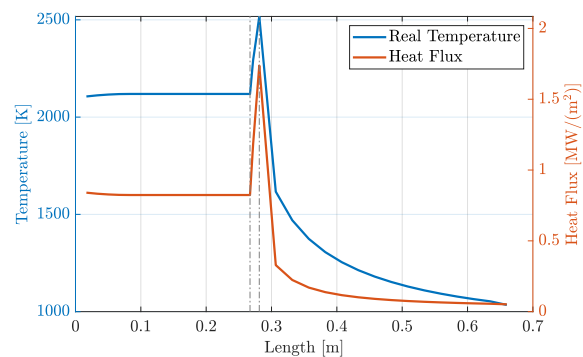


Figure 3.6: Wall temperature and heat flux - Green halved

In the case of the green halved, Figures 3.5 and 3.6, if the problem near the throat area is solved the coating together with the cooling system, could be enough to ensure the survivability of the wall, without damaging the coating. The same can be said for the case of the green nominal, Figures 3.7 and 3.8.

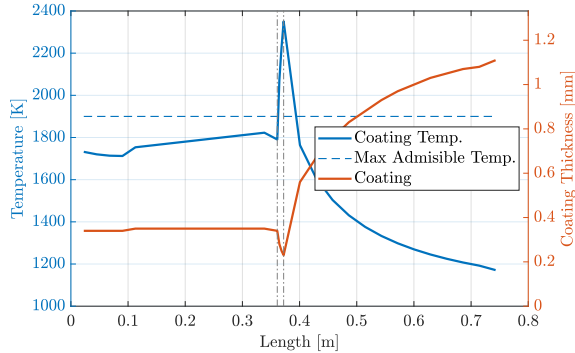


Figure 3.7: Coat temperature and thickness -
Green nominal

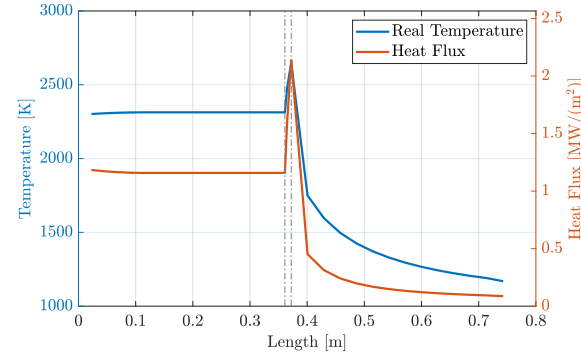


Figure 3.8: Wall temperature and heat flux -
Green nominal

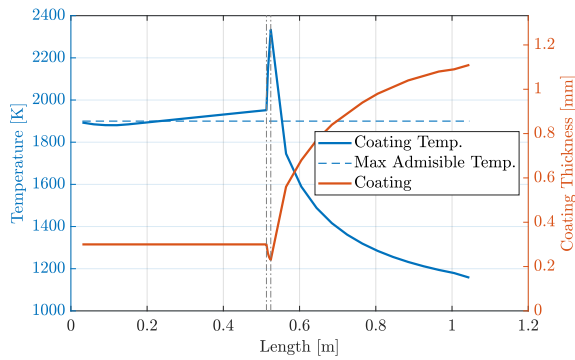


Figure 3.9: Coat temperature and thickness -
Green doubled

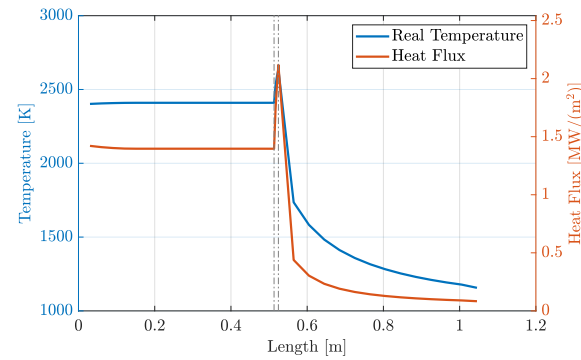


Figure 3.10: Wall temperature and heat flux -
Green doubled

The green double presents more challenges, as seen above in Figures 3.9 and 3.10. The temperatures of the coating are slightly higher than the maximum service temperature. Even though the mass flow rate of the coolant is much higher than in the toxic cases, this does not compensate the high convective heat coefficient of this couple of propellants. In fact, these engines have a coefficient that is almost double than the others. Therefore, a different approach for the cooling of the chamber and convergent would have to be considered. The nozzle could implement this kind of coating without a problem.

As it can be appreciated, the thickness of the coating in the divergent goes above 1 mm in all the cases studied, and the chosen coating goes above the maximum service temperature in the convergent area. To assess these problems, a multilayered coating could be applied [57], and a better implementation of the cooling jacket should be considered, but it goes beyond the scope of this paper.

Results and Conclusion

The design of the six different types of engine was carried out by trying to optimize the performances without compromising largely the total weight of the system. Considering that the thrust chamber of the engines had to be made with additive manufacturing, materials and dimensions compliant with this technology were chosen. This process led to the full sizing of the six engines, three of them using a rather common couple of propellants: MMH and N₂O₄; while the other three implement a less toxic option: HTP 98% and Kerosene. In the table below 3.2 the performances obtained from the numerical analysis are summarized.

	Halved		Nominal		Doubled	
	Green	Toxic	Green	Toxic	Green	Toxic
I_{sp} [s]	339	327	341	327	341	330
$I_{sp,VAC}$ [s]	347	334	350	334	350	336
A_e/A_t [-]	172	164	164	148	162	180
$\frac{O}{F}$ [-]	6.17	1.6	6.17	1.6	6.17	1.6
Inlet Press. [bar]	12	10.2	24	15	24	21.6
P_{CC} [bar]	10	8.5	20	12.5	20	18
T_{CC} [K]	3029	3019	3095	3046	3095	3071
T/W [-]	0.128	0.124	0.258	0.246	0.516	0.495
Total Mass [kg]	398	412	395	414	395	412
Injector	Triplet	Double Unlike	Triplet	Double Unlike	Triplet	Double Unlike
c^* [m/s]	1449	1490	1532	1507	1483	1518
C_F [-]	2.30	2.15	2.18	2.13	2.26	2.13

Table 3.2: Performance Datasheet comparison between the six final engines

The highest value of $I_{sp,VAC}$ is reached by the green doubled engine. The main drawback of this solution regards T_{flame} , which increases dramatically; therefore, a coating layer is required, additionally to the regenerative cooling system inside the combustion chamber and convergent section of the nozzle. This issue appears both in the doubled configuration and its nominal counterpart. The presence of the layer increases the complexity of the manufacturing, that has to be sprayed on the internal surface of the engine once the production is over.

An additional concern involves HTP 98% since it can dissociate in presence of Inconel 718 implying structural problems. For this reason, and to fulfill the need for high pressure levels inside tanks, the material chosen to store pressurizing gas, fuel and oxidizer is Titanium, for all cases. Since the selected $\frac{O}{F}$ for the green couple is 6.17, the volume of the oxidizer tank and the volume of its pressuring gas are twice the fuel ones. The value of $\frac{O}{F}$ also influences the configuration of the injectors, that are disposed on a triplet geometry. This does not imply feasibility problems linked to additive manufacturing.

The toxic cases have a lower $I_{sp,VAC}$; however, the nominal and large configurations do not need a coating layer to cool down the system. In terms of feasibility, the use of only additive manufacturing represents a simpler technological solution compared to the green engines. On the other hand, the values of dry mass, volumes of the propellant, and pressurizing tanks are higher.

Nevertheless, by considering combustion chamber and nozzle's masses, and the dry mass of the pressurizing systems, the 250 kg constraint on the dry mass is respected for all the six engine configurations.

In conclusion, if the main driver for the engine selection is the security and robustness of the systems, toxic propellants are the most desired. If, however, the main driving factor for the selection is the mass, volume and I_{sp} efficiency, then the green propellant couple is the most convenient. Moreover, if higher precision for the kick-stage is desired, compromising the higher thrust capability, regardless of propellant type, the halved thrust case is the most suitable.

Bibliography

- [1] Rocket Factory Augsburg. RFA One payload user guide. 07 2022.
- [2] Stefania Carlotti and Filippo Maggi. Evaluating new liquid storable bipropellants: Safety and performance assessments. *Aerospace*, 9(10), 2022.
- [3] Alberto Saritzu, Lily Blondel-Canepari, Riccardo Gelain, Patrick Hendrick, and Angelo Pasini. Trade-off study of green technologies for upper stage applications. *Space Propulsion Conference 2022*, 05 2022.
- [4] Chuang Zhou, Nanjia Yu, Tianwen Li, and Haojie Gong. A dual-mode hydrogen peroxide and kerosene space propulsion system pressurized by electric pumps. *Journal of Physics: Conference Series*, 2235(1):012079, may 2022.
- [5] I Yu, Tae Kim, Young Ko, Jun Jeon, and Sun Kim. Development and verification test of a bi-propellant thruster using hydrogen peroxide and kerosene. *International Journal of Aeronautical and Space Sciences*, 18:270–278, 06 2017.
- [6] G. Ngwu, B. Ugheoke, O. Yusuf, M. Nyabam, and S. Onuh. Numerical analysis and modelling of a 100 n hypergolic liquid bipropellant thruster. *Advances in Aerospace Science and Technology*, 5:85–99, 2020.
- [7] Sungkwon Jo, Sungyong An, Jonghak Kim, Hosung Yoon, and Sejin Kwon. Performance characteristics of hydrogen peroxide/kerosene staged-bipropellant engine with axial fuel injector. *Journal of Propulsion and Power*, 27:684–691, 05 2011.
- [8] Sen Li, Yifei Ge, Xiaolin Wei, and Teng Li. Mixing and combustion modeling of hydrogen peroxide/kerosene shear-coaxial jet flame in lab-scale rocket engine. *Aerospace Science and Technology*, 56:148–154, 2016.
- [9] Shinjae Kang. Catalyst bed behavior of hydrogen peroxide/kerosene bipropellant thruster in monopropellant and bipropellant modes with cavitating venturi valve. *Acta Astronautica*, 205:47–56, 2023.
- [10] Yang-Suk LEE and Jun Hwan Jang. The design and performance on 200n-class bipropellant rocket engine using decomposed h₂o₂ and kerosene. *INCAS BULLETIN*, 11:99–110, 09 2019.
- [11] Ian Coxhill, Guy Richardson, and Martin Sweeting. *An Investigation of a Low Cost HT-P/Kerosene 40 N Thruster for Small Satellites*.
- [12] Seonuk Heo, Sejin Kwon, and Sangwoo Jung. *Development of Hydrogen Peroxide/Kerosene 2,500 N Bipropellant Thruster for Long-term Operation by Film Cooling*.
- [13] Yu Cong, Tao Zhang, Tao Li, Jiwen Sun, Xiaodong Wang, Lei Ma, Dongbai Liang, and Liwu Lin. Propulsive performance of hypergolic h₂o₂/kerosene bipropellant. *Journal of Propulsion and Power*, 20(1):83–86, 2004.
- [14] Kamil M. Sobczak, Paweł Surmacz, Bartosz Bartkowiak, Adam Okninski, Grzegorz P. Rarata, Piotr Wolanski, Dominik Kublik, and Ferran Valencia Bel. *Test Campaign of a Green Liquid Bi-propellant Rocket Engine Using Catalytically Decomposed 98% Hydrogen Peroxide as Oxidizer*.

- [15] Adam Okninski, Jan Kindracki, and Piotr Wolanski. Multidisciplinary optimisation of bipropellant rocket engines using h₂o₂ as oxidiser. *Aerospace Science and Technology*, 82-83:284–293, 2018.
- [16] Eric Wernimont and Dick Durant. *Development of a 250 lbfv Kerosene - 90% Hydrogen Peroxide Thruster*.
- [17] Tim Dorau, Martin Propst, Samira Gruber, Alex Selbmann, Adheena Joseph, Jan Sieder-Katzmann, Maximilian Buchholz, Kamil Sobczak, Sebastian Soller, Martin Tajmar, and Christian Bach. Development of an additively manufactured hydrogen peroxide / kerosene 6kn aerospike breadboard engine. 10 2021.
- [18] J.A. Smith R.C. Stechman. Liquid rocket propellants. *Encyclopedia of Physical Science and Technology*, 3, 2003.
- [19] J.A. Smith R.C. Stechman. Monomethyl hydrazine vs. hydrazine fuels: Test results using flight qualified 100 lbf and 5 lbf bipropellant engine configurations. *19th Joint Propulsion Conference*, 1983.
- [20] Nammo. Leros 4 interplanetary engine.
- [21] Aerojet Rocketdyne. In-space propulsion data sheet.
- [22] Sebastian Soller, R Behr, S Beyer, F Laithier, M Lehmann, A Preuss, and R Salapete. Design and testing of liquid propellant injectors for additive manufacturing. *European Conference on Aerospace Sciences (EUCASS)*, 07 2017.
- [23] Sebastian Soller, S Beyer, A Dahlhaus, A Konrad, J Kretschmer, N Rackemann, and W Zeiss. Development of liquid rocket engine injectors using additive manufacturing. *European Conference for Aeronautics and Space Science*, 07 2015.
- [24] Sebastian Soller, Alexandre Barata, Steffen Beyer, Arne Dahlhaus, Didier Guichard, Erwan Humbert, Joachim Kretschmer, and Wilke Zeiss. Selective laser melting (slm) of inconel 718 and stainless steel injectors for liquid rocket engines. *Space Propulsion Conference 2016*, 05 2016.
- [25] Cagri Oztan and Victoria Coverstone. Utilization of additive manufacturing in hybrid rocket technology: A review. *Acta Astronautica*, 180:130–140, 2021.
- [26] EOS GmbH Electro Optical Systems. Eos nickelalloy in718 material data sheet. *Metal Solutions*, 2023.
- [27] Tyler R. Kakuda, Andi M. Limarga, Ted D. Bennett, and David R. Clarke. Evolution of thermal properties of eb-pvd 7ysz thermal barrier coatings with thermal cycling. *Acta Materialia*, 57, 2009.
- [28] Ansys. Granta edupack. *Materials*, 2023.
- [29] Chemical and Material Sciences Department Research Division. *Hydrogen Peroxide Handbook*. Rocketdyne, 1967.
- [30] Matteo Fagherazzi, Marco Santi, Francesco Barato, and Daniele Pavarini. Design and testing of a 3d printed regenerative cooled nozzle for a hydrogen peroxide based bi-propellant thruster. *AIAA Propulsion and Energy 2021 Forum*, 2021.

- [31] Chemical and Material Sciences Department Research Division. Hydrogen peroxide handbook. *Rocketdyne, a Division of North American Aviation, Inc.*, 1967.
- [32] Chemical and Material Sciences Department Research Division. An investigation of a low cost bi-propellant rocket engine for small satellites. *University of Surrey*, 2002.
- [33] Grzegorz Rarata and Paweł Surmacz. The safe preparation of htp and concentrated h₂o₂ samples. *PRACE INSTYTUTU LOTNICTWA*, 01 2011.
- [34] John A. Halchak, James L. Cannon, and Corey Brown. Materials for liquid propulsion systems. *NASA Marshall Space Flight Center, Aerojet-Rocketdyne*, 2018.
- [35] Dtic ad0866010: Materials compatibility with liquid rocket propellants : Defense technical information center : Free download, borrow, and streaming, Feb 1970.
- [36] P. E. Uney and D. A. Fester. Material compatibility with space storable propellant. *Jet Propulsion Laboratory, California Institute of Technology*, 1972.
- [37] Propellant material compatibility program and results - nasa technical reports server (ntrs), Aug 1976.
- [38] Material compatibility with space storable propellants. design guidebook - nasa technical reports server (ntrs), Mar 1972.
- [39] Raymond C. Benn and Randy P. Salva. Additively manufactured inconel® alloy 718. *7th international symposium on superalloy 718 and its derivatives, TMS (The Minerals, Metals and Materials Society)*, 2010.
- [40] SLM Solutions Group AG. Slm 800 brochure. *Large Format Selective Laser Melting*, 2023.
- [41] Alexander Paolini, Stefan Kollmannsberger, and Ernst Rank. Additive manufacturing in construction: A review on processes, applications, and digital planning methods. *Additive Manufacturing*, 30, 2019.
- [42] Srishti Jain, Mike Corliss, Bruce Tai, and Wayne Nguyen Hung. Electrochemical polishing of selective laser melted inconel 718. *Procedia Manufacturing*, 34, 2019.
- [43] Jagmit Singh, Luis Zerpa, Benjamin Partington, and Jose Gamboa. Effect of nozzle geometry on critical-subcritical flow transitions. *Heliyon*, 5:e01273, 02 2019.
- [44] Filippo Maggi. Lecture notes. *Space Propulsion*, 2022 - 2023.
- [45] Shuaijie Xue, Weidong Yang, Lixin Zhou, and Hongjun Liu. Experimental investigation of self-excited combustion instabilities in a small earth storable bipropellant rocket combustor. *Aerospace Science and Technology*, 105:106008, 2020.
- [46] S.D. Heister, W.E. Anderson, T.L. Pourpoint, and R.J. Cassady. *Rocket Propulsion*. Cambridge Aerospace Series. Cambridge University Press, 2019.
- [47] Mangesh Nadkarni, Rohan Mehta, Ritesh Sarode, Suraj Ghadge, and Ganesh Karpe. Design of pressure vessel for nitrogen gas storage. *International Journal of Advance Research in Science and Engineering*, 03 2018.
- [48] A. Cervone K. V. Man, F. Topputo. Chemical propulsion system design for a 16u interplanetary cubesat. *69th International Astronautical Congress*, 2018.

- [49] Moog. Torque motor latch valve (tmlv). *Moog space and defense group*, 2023.
- [50] J. J. Hansen, M. Hussein, S. Moehring, M. Stauffer, C. Acosta, and P. Imper J. Daly, N. Chennoju. Student design of a bipropellant liquid rocket engine and associated infrastructure. *AIAA 2020-3918 Session: Propulsion Education III - Student Research Projects*, 2020.
- [51] S. Kang. Catalyst bed behavior of hydrogen peroxide/kerosene bipropellant thruster in monopropellant and bipropellant modes with cavitating venturi valve. *Acta astronautica*, 2023.
- [52] P. Eckart, S. Angelucci, L. Appolloni, H. Baier, M. Canales, A. da Silva-Curiel, E. Freidl, E. Igenbergs, M. Kesselmann, T. Neff, K. Pauly, T. Pühlhofer, F. Schlerka, W. Seefelder, L. Tarabini, A. Straub, and S. Ullmann. Microspacecraft platform with bipropellant propulsion system and 3-axis stabilization for missions in earth orbit and beyond leo. *14th Annual / USU Conference on Small Satellites*, 2000.
- [53] Charlie Taylor. Mmh. *Rocket Props*, 2023.
- [54] C. C. Lin, F. R. Smith, N. Ichikawa, T. Baba, and M. Itow. Decomposition of hydrogen peroxide in aqueous solutions at elevated temperatures. *International Journal of Chemical Kinetics*, 23(11):971–987, 1991.
- [55] Antonio Salerno. Lecture notes. *Fisica Tecnica*, 2020 - 2021.
- [56] Manfredo Gherardo Guilizzoni. Lecture notes. *Heat Transfer and Thermal Analysis*, 2022 - 2023.
- [57] Xiaoying Zhang. Coupled simulation of heat transfer and temperature of the composite rocket nozzle wall. *Aerospace Science and Technology*, 15(5):402–408, 2011.

Appendix A

CAD Modelling

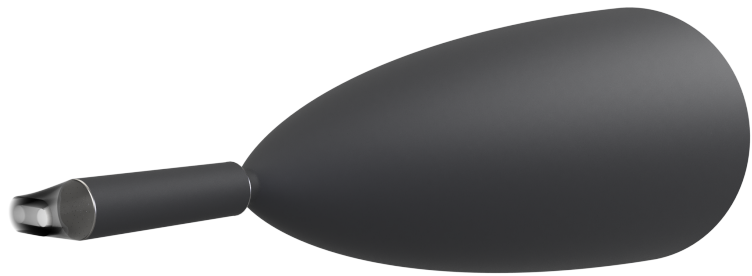


Figure A.1: CAD model of the Toxic Nominal engine



Figure A.2: Cutaway CAD model of the Toxic Nominal engine



Figure A.3: CAD model of the Green Nominal engine

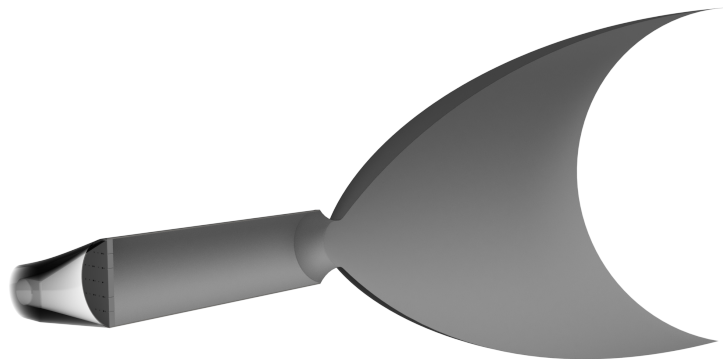


Figure A.4: Cutaway CAD model of the Green Nominal engine

Appendix B

Graphical Approaches

B.1 Rao Approximation

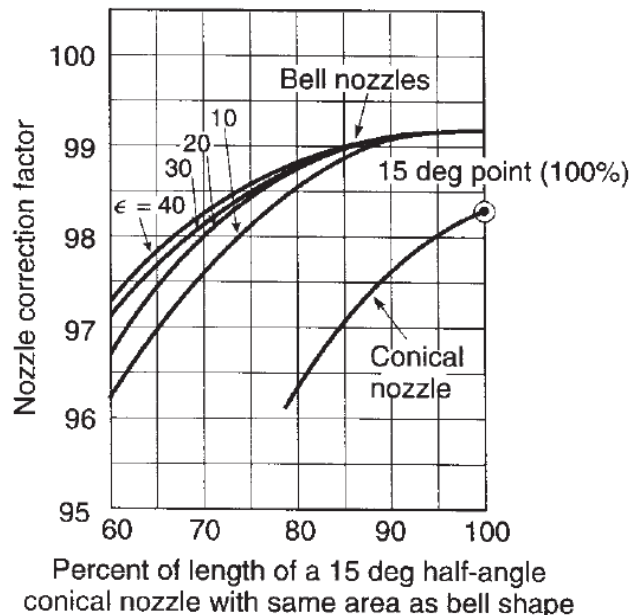


Figure B.1: Efficiency of an equivalent bell nozzle as a function of percentage of an equivalent 15 deg conical nozzle

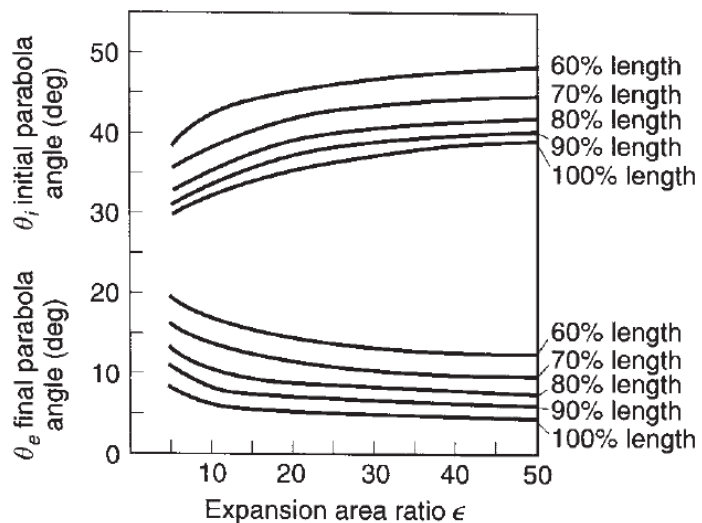


Figure B.2: Limit parabola angles of an equivalent bell nozzle as a function of expansion ratio and percentage of an equivalent 15 deg conical nozzle

Appendix C

CEAM Analysis

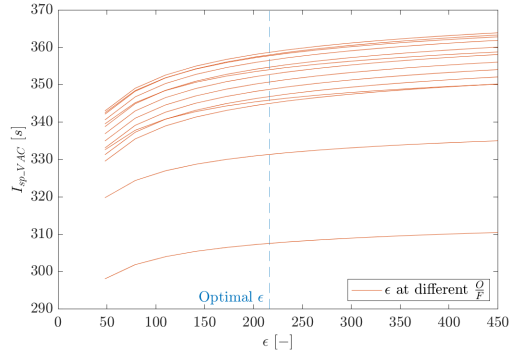


Figure C.1: Green nominal - ϵ at different $\frac{O}{F}$

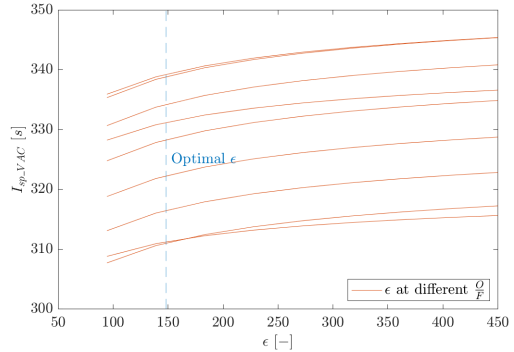


Figure C.2: Toxic nominal - ϵ at different $\frac{O}{F}$

Used CEAM Data						
	Green halved	Green nominal	Green doubled	Toxic halved	Toxic nominal	Toxic doubled
ρ [kg/m^3]	0.8237	1.6234	1.6234	0.6830	0.9978	1.4284
M_{mol} [kg/mol]	0.0207	0.0209	0.0209	0.0202	0.0202	0.0203
T_{flame} [K]	3029.4	3094.5	3094.5	3019.3	3046.6	3071.1
h [kJ/kg]	-3846.5	-3846.5	-3846.5	335.1	335.1	335.1
C_p [-]	7.4242	6.7719	6.7719	4.3374	4.0821	3.8610
γ [-]	1.0571	1.0625	1.0625	1.1050	1.1120	1.1189
μ [Pa/s]	0.0103	0.0105	0.0105	0.0094	0.0095	0.0095

Table C.1: Used CEAM's results

C.1 Chemical Composition At Exit Section

Green Couple - Nominal Thrust	
Element	Molar Fraction
CO	0.09156
CO ₂	0.11685
H	0.01210
HO ₂	0.00004
H ₂	0.06666
H ₂ O	0.64566
H ₂ O ₂	0.00001
O	0.00457
OH	0.04514
O ₂	0.01741

Table C.2: Chemical composition at the exit of the nozzle for the green couple in nominal condition

Toxic Couple - Nominal Thrust	
Element	Molar Fraction
CO	0.18690
CO ₂	0.07373
H	0.00106
H ₂	0.01689
H ₂ O	0.28414
NO	0.00282
N ₂	0.41989
O	0.00082
OH	0.01249
O ₂	0.00122

Table C.3: Chemical composition at the exit of the nozzle for the toxic couple in nominal condition

Green Couple - Half Thrust	
Element	Molar Fraction
CO	0.09363
CO ₂	0.11342
H	0.01449
HO ₂	0.00004
H ₂	0.07021
H ₂ O	0.63456
H ₂ O ₂	0.00001
O	0.00558
OH	0.04816
O ₂	0.01990

Table C.4: Chemical composition at the exit of the nozzle for the green couple in halved condition

Toxic Couple - Half Thrust	
Element	Molar Fraction
CO	0.18689
CO ₂	0.07376
H	0.00118
H ₂	0.01690
H ₂ O	0.28234
NO	0.00301
N ₂	0.41981
O	0.00101
OH	0.01361
O ₂	0.00149

Table C.5: Chemical composition at the exit of the nozzle for the toxic couple in halved condition

Green Couple - Double Thrust	
Element	Molar Fraction
CO	0.09156
CO ₂	0.11685
H	0.01210
HO ₂	0.00004
H ₂	0.06666
H ₂ O	0.64566
H ₂ O ₂	0.00001
O	0.00457
OH	0.04514
O ₂	0.01741

Table C.6: Chemical composition at the exit of the nozzle for the green couple in doubled condition

Toxic Couple - Double Thrust	
Element	Molar Fraction
CO	0.18690
CO ₂	0.07373
H	0.00095
H ₂	0.01688
H ₂ O	0.28578
NO	0.00263
N ₂	0.41998
O	0.00067
OH	0.01145
O ₂	0.00101

Table C.7: Chemical composition at the exit of the nozzle for the toxic couple in doubled condition

C.2 Equilibrium, Frozen and Bray Models

C.2.1 Nominal Case

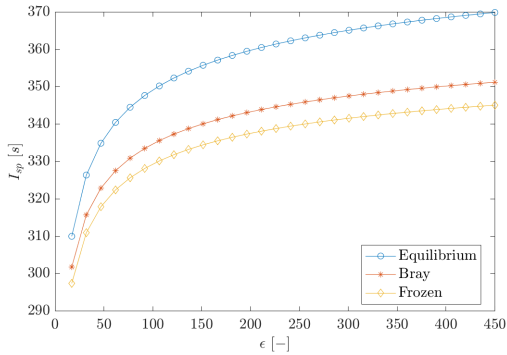


Figure C.3: Green nominal - ϵ vs I_{sp}

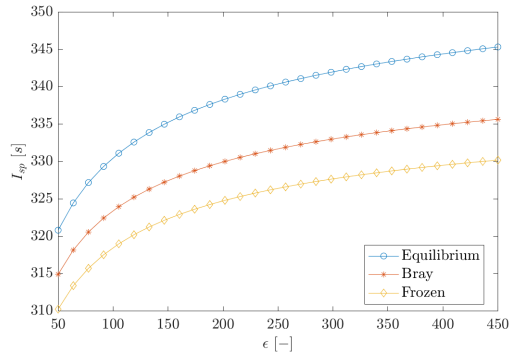


Figure C.4: Toxic nominal - ϵ vs I_{sp}

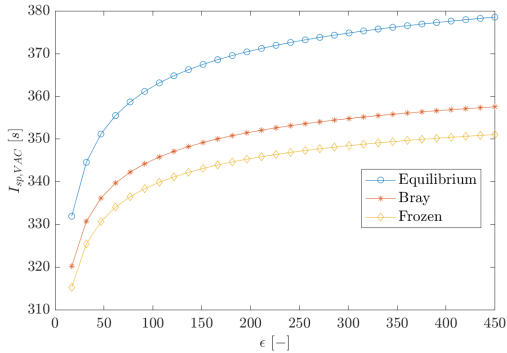


Figure C.5: Green nominal - ϵ vs I_{sp_VAC}

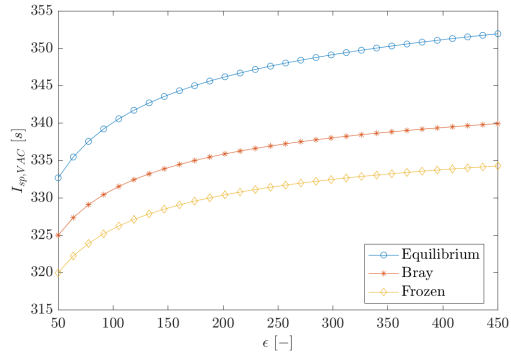


Figure C.6: Toxic nominal - ϵ vs I_{sp_VAC}

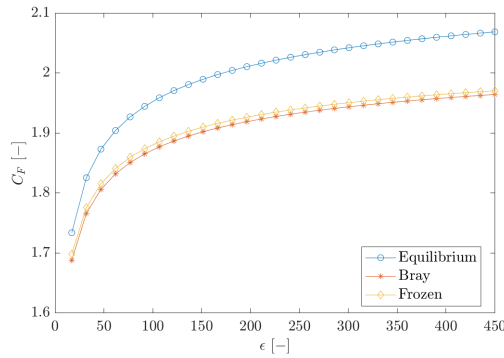


Figure C.7: Green nominal - ϵ vs C_F

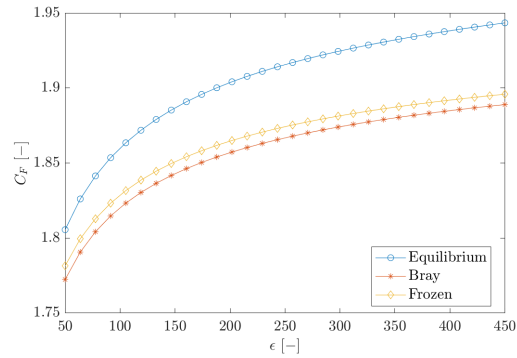


Figure C.8: Toxic nominal - ϵ vs C_F

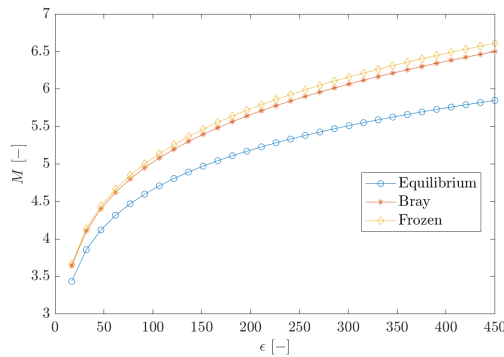


Figure C.9: Green nominal - ϵ vs M

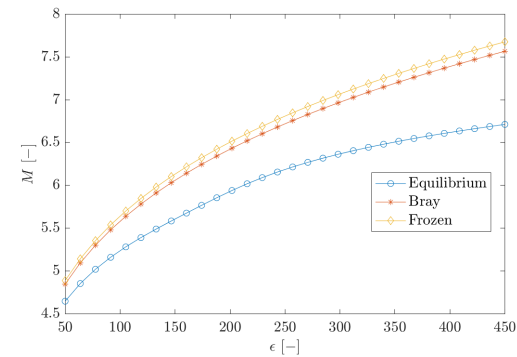


Figure C.10: Toxic nominal - ϵ vs M

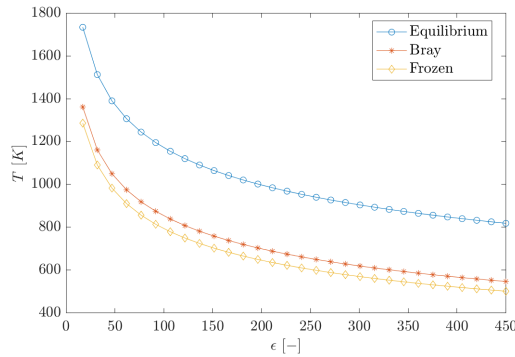


Figure C.11: Green nominal - ϵ vs T

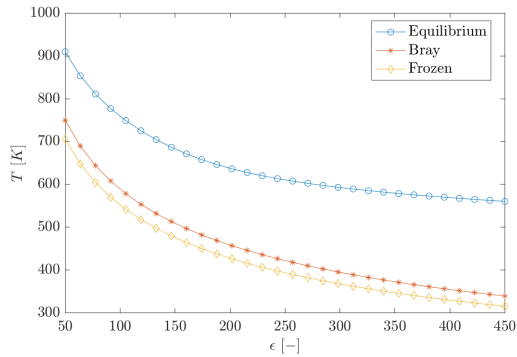


Figure C.12: Toxic nominal - ϵ vs T

C.2.2 Halved Case

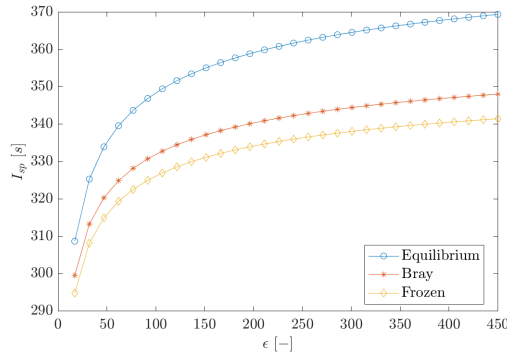


Figure C.13: Green halved - ϵ vs I_{sp}

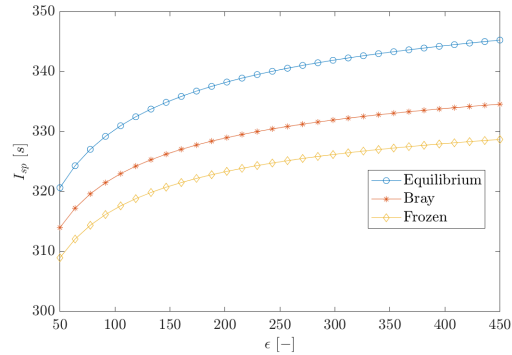


Figure C.14: Toxic halved - ϵ vs I_{sp}

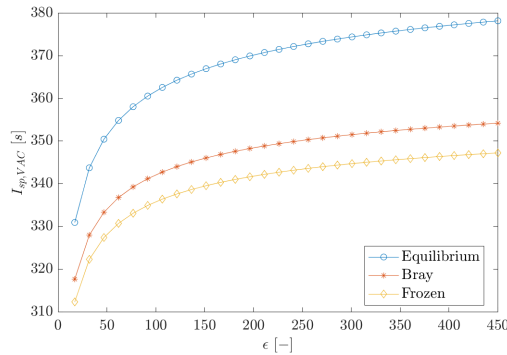


Figure C.15: Green halved - ϵ vs I_{sp_VAC}

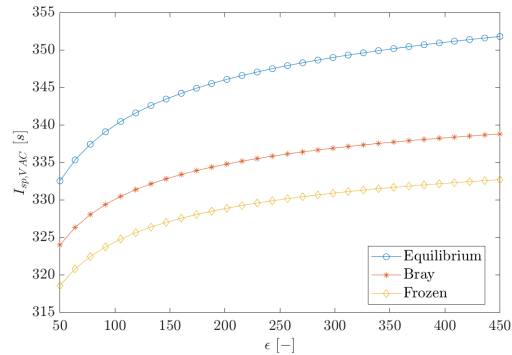


Figure C.16: Toxic halved - ϵ vs I_{sp_VAC}

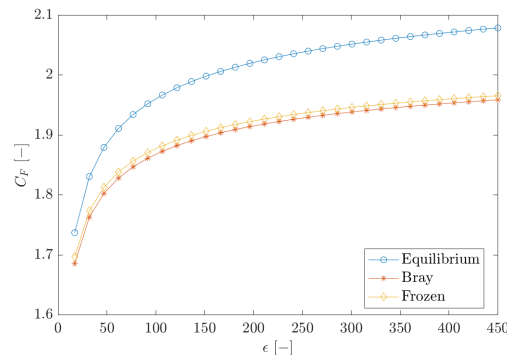


Figure C.17: Green halved - ϵ vs C_F

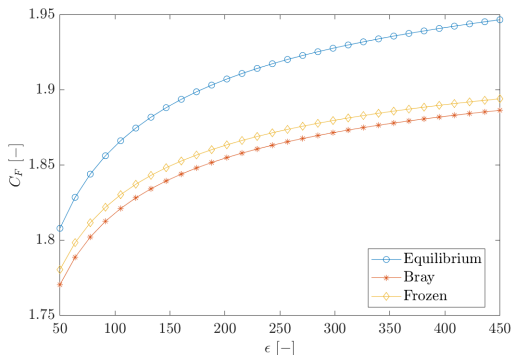


Figure C.18: Toxic halved - ϵ vs C_F

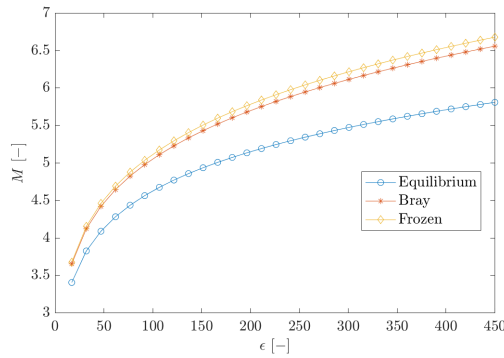


Figure C.19: Green halved - ϵ vs M

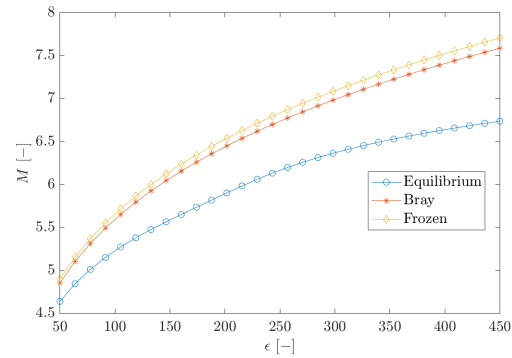


Figure C.20: Toxic halved - ϵ vs M

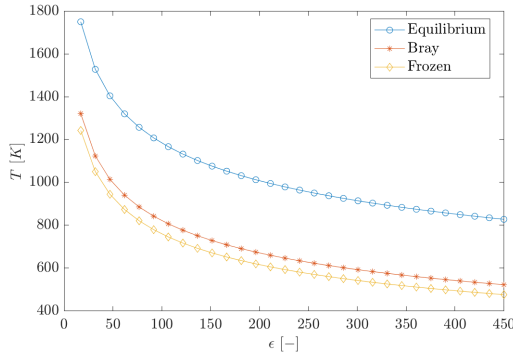


Figure C.21: Green halved - ϵ vs T

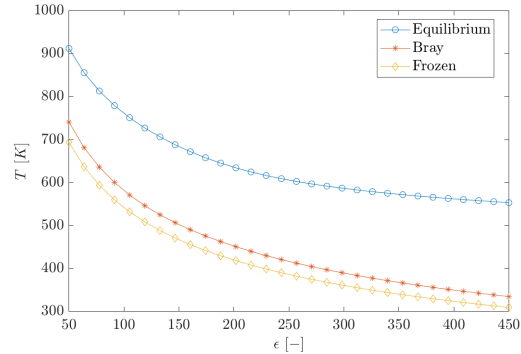


Figure C.22: Toxic halved - ϵ vs T

C.2.3 Doubled Case

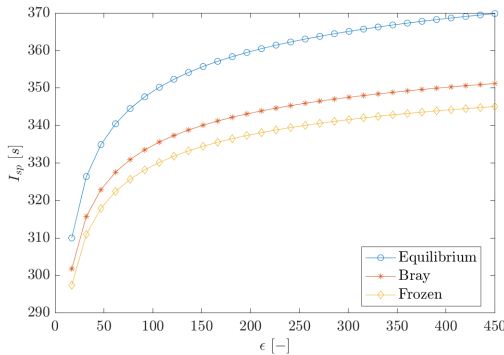


Figure C.23: Green doubled - ϵ vs I_{sp}

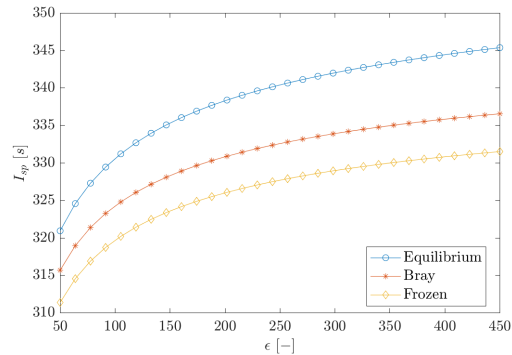


Figure C.24: Toxic doubled - ϵ vs I_{sp}

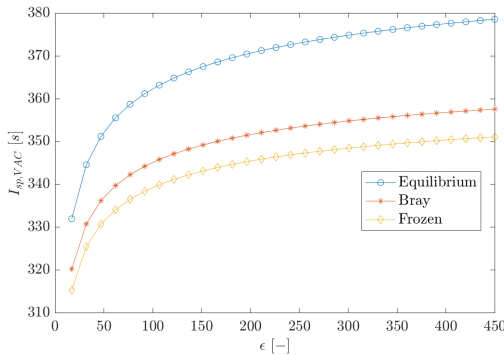


Figure C.25: Green doubled - ϵ vs $I_{sp\text{-}VAC}$

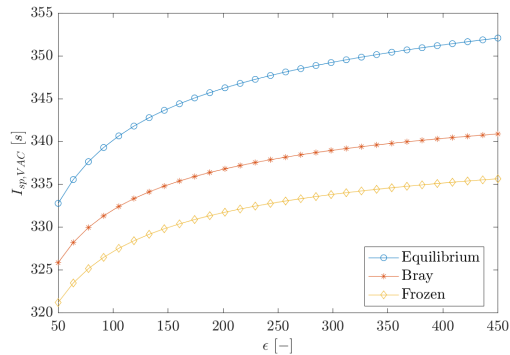


Figure C.26: Toxic doubled - ϵ vs $I_{sp\text{-}VAC}$

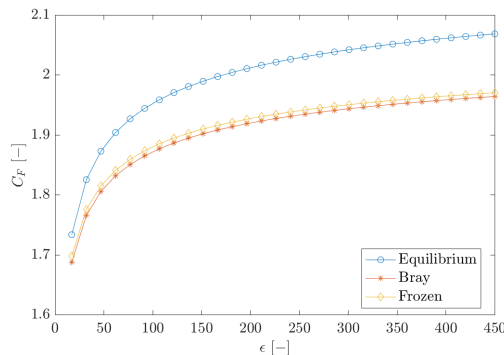


Figure C.27: Green doubled - ϵ vs C_F

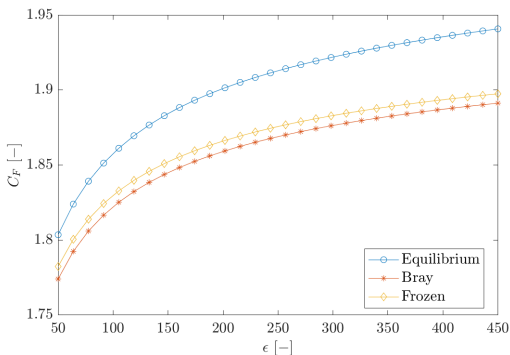


Figure C.28: Toxic doubled - ϵ vs C_F

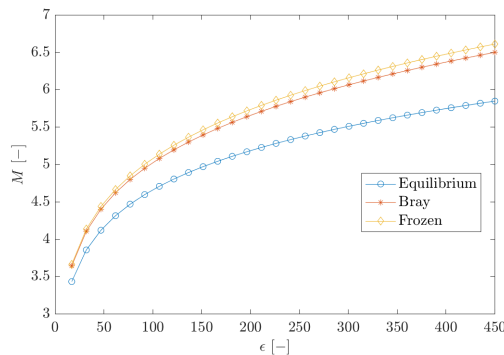


Figure C.29: Green doubled - ϵ vs M

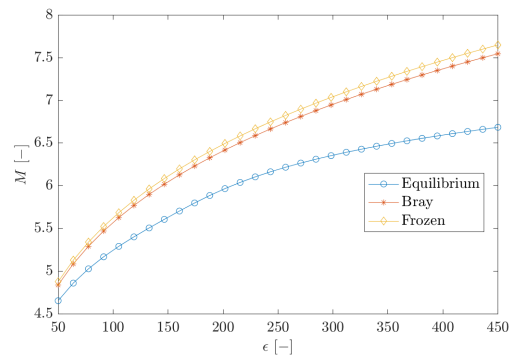


Figure C.30: Toxic doubled - ϵ vs M

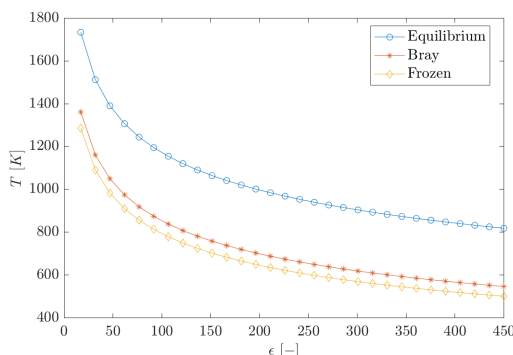


Figure C.31: Green doubled - ϵ vs T

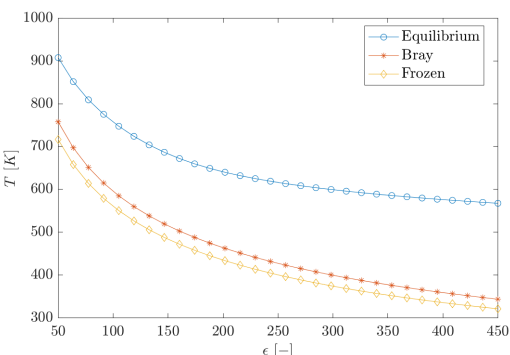


Figure C.32: Toxic doubled - ϵ vs T

Appendix D

Pressure cascade: full analysis

A full analysis of the remaining 5 pressure cascades is reported

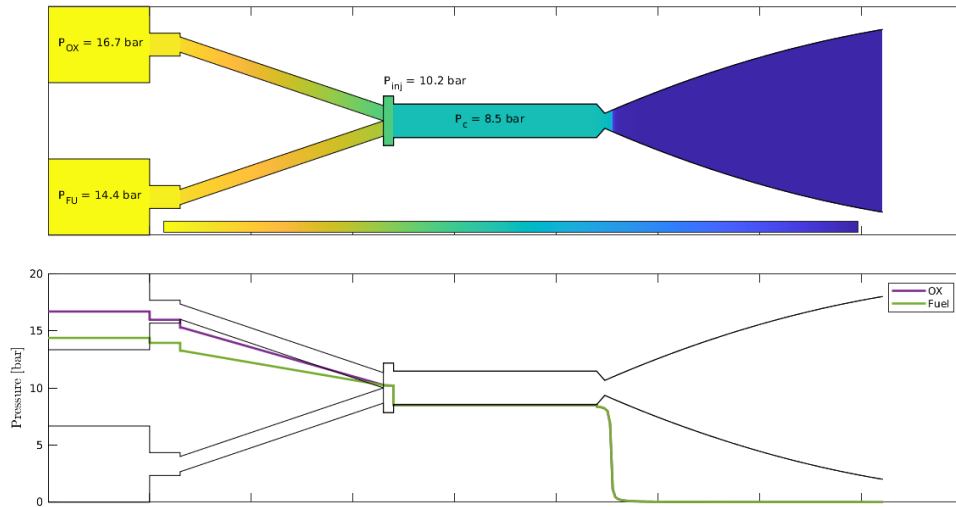


Figure D.1: Pressure cascade - Toxic halved

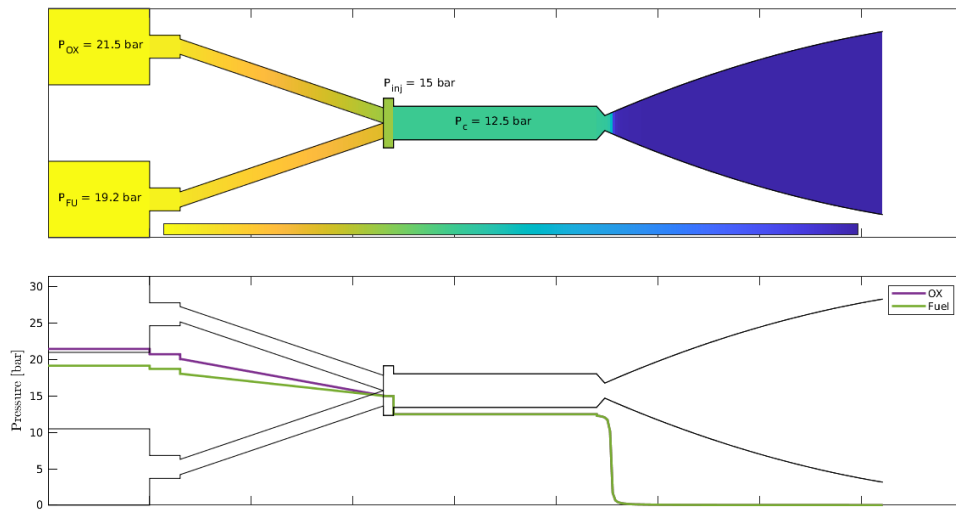


Figure D.2: Pressure cascade - Toxic nominal

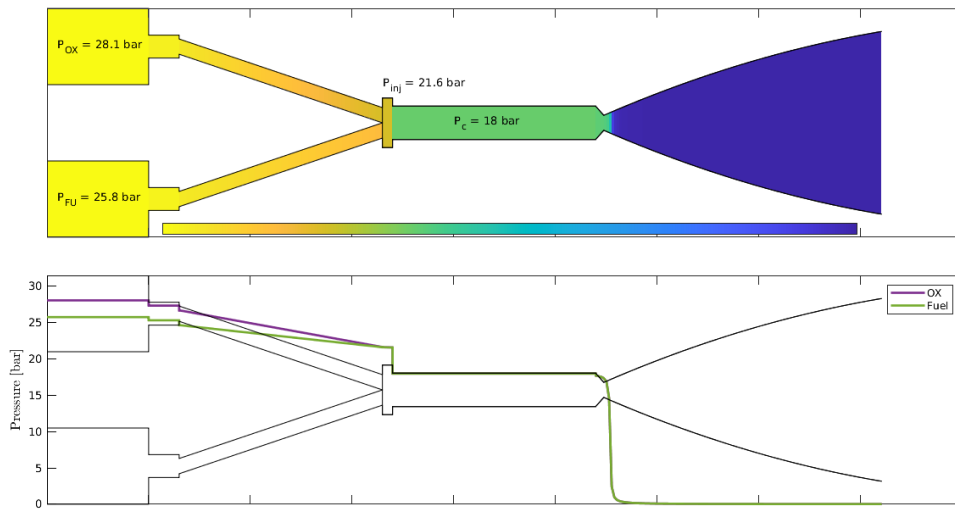


Figure D.3: Pressure cascade - Toxic doubled

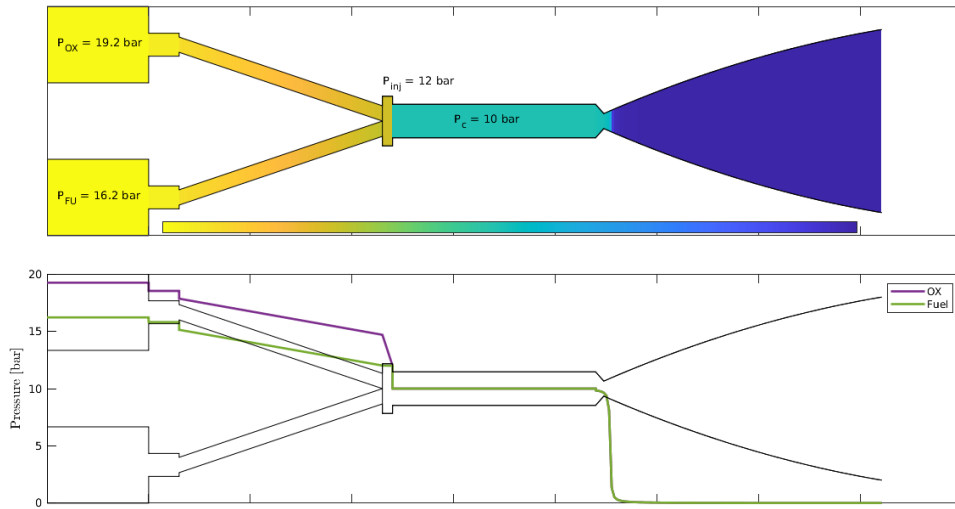


Figure D.4: Pressure cascade - Green halved

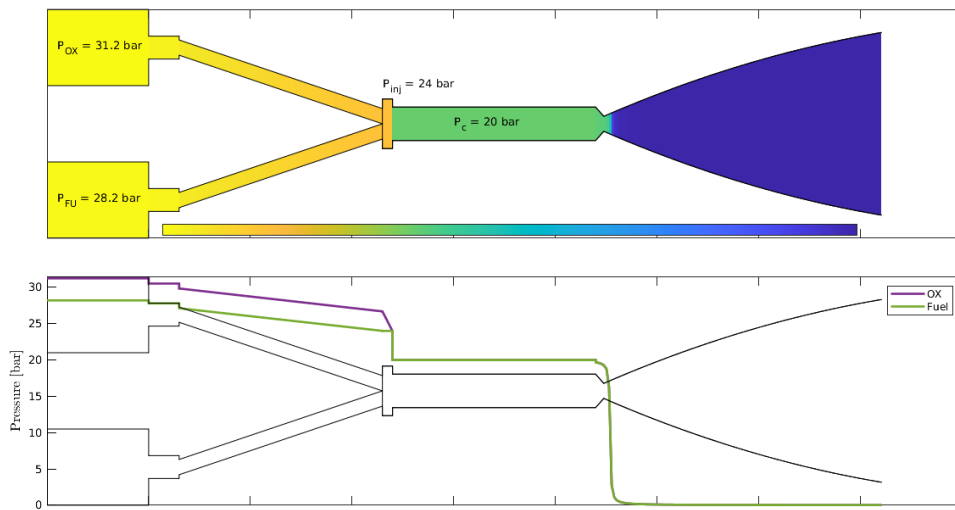


Figure D.5: Pressure cascade - Green doubled